

Structural Properties of the Sliding Columnar Phase in Layered Liquid Crystalline Systems

L. Golubović^{1,*}, T. C. Lubensky², and C. S. O'Hern^{2,†}

¹ *Department of Physics, Harvard University, Cambridge, MA 02138*

² *Department of Physics and Astronomy, University of Pennsylvania, Philadelphia, PA 19104-6396*
(November 2, 2018)

Under appropriate conditions, mixtures of cationic and neutral lipids and DNA in water condense into complexes in which DNA strands form local 2D smectic lattices intercalated between lipid bilayer membranes in a lamellar stack. These lamellar DNA-cationic-lipid complexes can in principle exhibit a variety of equilibrium phases, including a columnar phase in which parallel DNA strands form a 2D lattice, a nematic lamellar phase in which DNA strands align along a common direction but exhibit no long-range positional order, and a possible new intermediate phase, the sliding columnar (SC) phase, characterized by a vanishing shear modulus for relative displacement of DNA lattices but a nonvanishing modulus for compressing these lattices. We develop a model capable of describing all phases and transitions among them and use it to calculate structural properties of the sliding columnar phase. We calculate displacement and density correlation functions and x-ray scattering intensities in this phase and show, in particular, that density correlations within a layer have an unusual $\exp(-\text{const.} \ln^2 r)$ dependence on separation r . We investigate the stability of the SC phase with respect to shear couplings leading to the columnar phase and dislocation unbinding leading to the lamellar nematic phase. For models with interactions only between nearest neighbor planes, we conclude that the SC phase is not thermodynamically stable. Correlation functions in the nematic lamellar phase, however, exhibit SC behavior over a range of length scales.

Pacs: 61.30.Cz, 61.30.Jf, 64.70.Md

I. INTRODUCTION

The search for non-viral vectors for transport of DNA across cell and nuclear membranes in gene therapy has led to the study of DNA-cationic-lipid complexes [1]. DNA and mixtures of neutral (zwitterionic) and cationic lipids dispersed in water self-assemble into spheroidal complexes that can attain micron sizes near the isoelectric point where there is compensation between DNA and lipid charge. Fluorescence tagging of DNA and lipids indicate [2] that both species are dispersed uniformly throughout the complexes. X-ray scattering experiments reveal two bulk structures [2–5] for the complexes with close association between DNA and lipids. When helper lipids that favor spontaneous curvature of lipid membranes or that decrease membrane charge density are added, a hexagonal inverted micellar structure forms with DNA molecules captured in the water holes of the hexagonal lattice [5]. When only neutral and cationic lipids are used, DNA is intercalated in galleries between lamellae of a lamellar lyotropic phase formed by the lipids [2–4] as depicted schematically in Fig. 1. This article will investigate the possible equilibrium phases of these lamellar DNA lipid complexes. It will focus primarily on the properties of one phase, the sliding columnar phase [6,7], characterized by strong orientational but weak positional correlation between DNA strands in neighboring galleries.

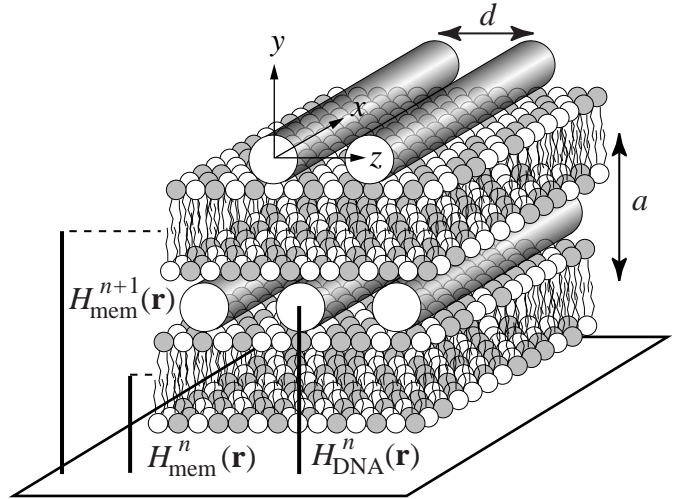


FIG. 1. Schematic representation of lamellar DNA-cationic-lipid complexes. Parallel strands of DNA form 2D smectic lattices with lattice spacing d in galleries between flat lipid bilayer membranes with spacing a . DNA strands are aligned parallel to the x axis and the y axis is normal to the lipid planes. The height of the midpoint of the n th membrane above a point $\mathbf{r} = (x, z)$ in the xz -plane is $H_{\text{mem}}^n(\mathbf{r})$. The n th DNA gallery with height $H_{\text{DNA}}^n(\mathbf{r})$ lies between the n th and the $n+1$ st membrane [See. Eqs. (2.1) and (2.2)].

DNA molecules are semi-flexible polymers that when confined to a two-dimensional plane tend to form locally

aligned structures with a preferred inter-molecular separation that can be modeled as two-dimensional smectic liquid crystals [8–10]. Thus, lamellar DNA-lipid complexes can be viewed as a 3D stack of 2D smectics as depicted in Fig. 1. This figure establishes the coordinate conventions that will be used throughout this paper. DNA strands align on average along the x direction, and the normal to lamellae is along the y axis. The normal to the 2D smectic lattices is along the z direction. The average spacing between lamellae is a , and that between DNA strands is d . The wavenumbers associated with these lengths are, respectively, $k_0 = 2\pi/a$ and $q_0 = 2\pi/d$.

If the lamellae are assumed not to be disrupted by dislocations or rips, then the following possible equilibrium phases are easily identified:

- **Columnar (C) Phase:** In this phase, DNA strands are aligned on average along the x axis, and their centers occupy positions on a 2D crystal lattice in the yz plane. Since the standard Coulomb repulsion between DNA strands favors staggering of smectic lattices in neighboring galleries, the columnar lattice is normally expected to be centered rectangular as observed in experiments on complexes in which membranes are in the $L_{\beta'}$ phase rather than the more disordered L_{α} phase [4]. We will, however, consider both simple rectangular and centered rectangular columnar lattices. A simple rectangular lattice may occur if the effective interaction between DNA strands in *different* galleries is attractive, as is the case between DNA strands in solutions with polyvalent salts [11]. The Columnar phase is favored at low temperature. It has the same symmetry as a columnar discotic liquid crystal phase [12]. It is characterized by a 2D elastic energy with a nonvanishing shear modulus for relative displacements of DNA lattices in different galleries and nonvanishing moduli for compression of both lamellae and DNA smectic lattices. It has long-range positional order in the 2D yz -plane and associated Bragg peaks in its x-ray scattering profile at reciprocal lattices vectors $\mathbf{G}_{m_1, m_2} = [0, m_1 k_0/2, m_2 q_0] \equiv (m_1, m_2)$ where m_1 and m_2 are integers and m_1 is even for a simple rectangular lattice and $m_1 + m_2$ is even for a centered rectangular lattice as shown Fig. 2.
- **Nematic Lamellar (NL) Phase:** In this phase, the periodic positional order of the columnar phase is destroyed by dislocations in the DNA smectic lattices, but the long-range orientational order of DNA strands is maintained. This phase is characterized by a long-wavelength elastic energy with a lamellar compression modulus, an anisotropic lamellar bending modulus, and orientational rigidities (Frank elastic constants) opposing spatially dependent variation of DNA alignment direction. Both the shear modulus for relative displacement

of DNA lattices in different galleries and the compression modulus for DNA lattices vanish, and there is exponential decay of DNA positional correlations. The x-ray scattering profile of the NL phase exhibits lamellar power-law $(2l, 0)$ peaks at $\mathbf{G}_{2l, 0} = (0, lk_0, 0)$. If columnar-phase positional correlations are well developed, it will also exhibit Lorentzian peaks at \mathbf{G}_{m_1, m_2} for $m_2 \neq 0$ as depicted in Fig. 2. If thermal fluctuations are sufficiently strong that these correlations are not well developed in centered rectangular systems, then the x-ray scattering profile could exhibit a broad $(0, 1)$ peak in the vicinity of $(0, 0, q_0)$ rather than the expected pair of $(1, 1)$ and $(-1, 1)$ peaks. In this case, the positions of the x-ray scattering peaks would appear to indicate a tendency to form a simple rectangular rather than the ground-state centered rectangular structure.

- **Isotropic Lamellar (IL) Phase:** In this phase, orientational as well as positional order of DNA lattices is lost. Macroscopically this phase is identical to a multi-component isotropic lamellar phase. It is included for completeness and will not be considered further in this paper.
- **Decoupled 2D Smectic (DS) Phase:** This phase occurs only if there are absolutely no interactions between DNA lattices in neighboring galleries. Its elasticity and correlations are thus those of independent 2D smectic lattices. Since there are always interactions between galleries, this phase will not exist in real systems. It is, however, a useful limit to consider since systems with weak coupling between layers will behave as though they are decoupled at sufficiently short length scales.

In addition to the above phases, which are straightforward to identify, there is the possibility of another phase with unusual properties:

- **Sliding Columnar (SC) Phase [6,7]:** This phase has properties intermediate between those of the columnar and lamellar nematic phases. Its elastic energy is distinguished from that of the NL phase by the presence of a nonvanishing modulus for compression of DNA lattices. In-plane smectic correlations die off as $\exp(-\text{const.} \ln^2 r)$ as a function of separation r rather than exponentially as in the NL phase. Correlations between smectic lattices in different galleries die off exponentially with layer-number difference. The x-ray structure factor exhibits power-law lamellar $(0, lk_0, 0)$ peaks and well defined DNA (m_1, m_2) peaks with $m_2 \neq 0$ that are sharper than the corresponding Lorentzian peaks in the NL phase, as depicted in Fig. 2. As in the NL phase, $(1, 1)$ and $(-1, 1)$ peaks may merge to produce a single $(0, 1)$ DNA peak if thermal fluctuations are sufficiently strong.

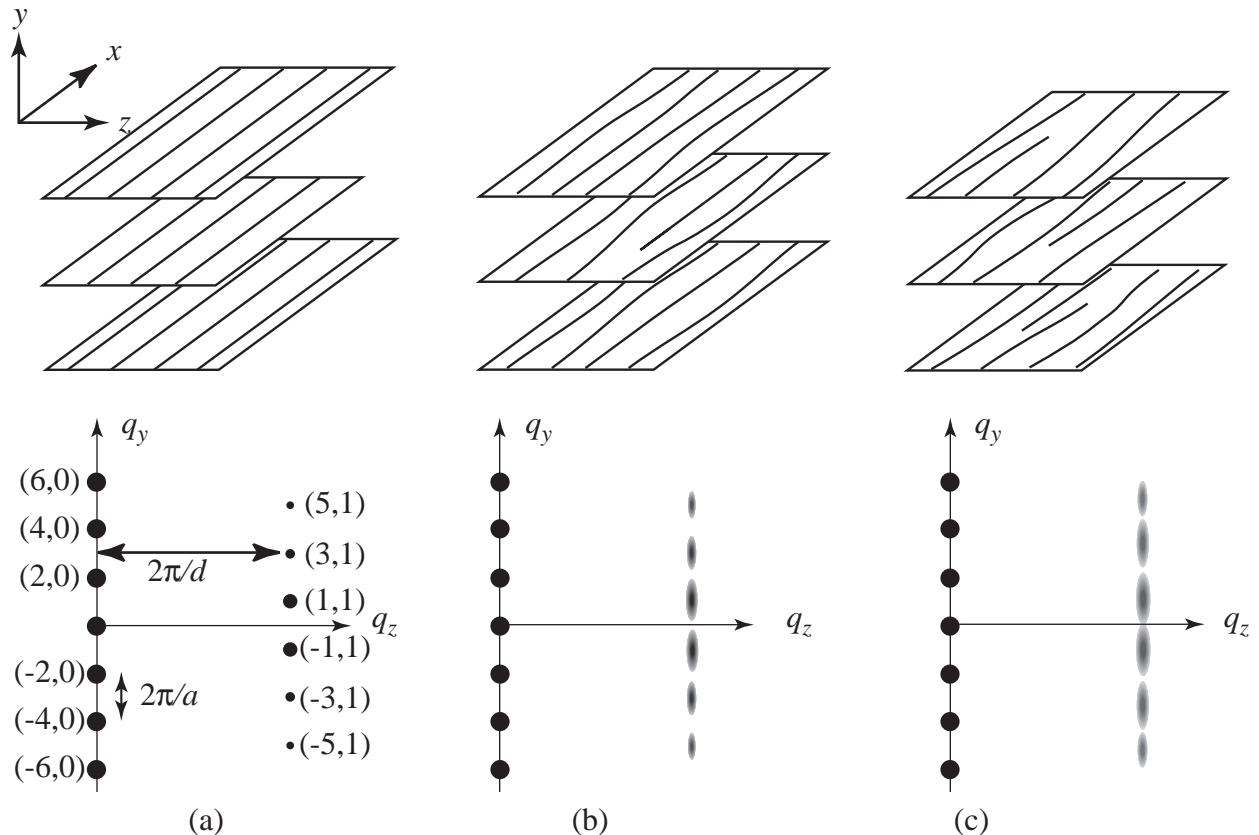


FIG. 2. Schematic representation of structure (top) and x-ray scattering profiles (bottom) of (a) the Columnar phase, (b) the Sliding Columnar phase, and (c) the Nematic Lamellar Phase. These figures assume that the preferred low-temperature phase is the centered-rectangular columnar phase. Modifications for a rectangular columnar phase are obvious. The indexing scheme for the x-ray intensities is the standard one for centered rectangular lattice. There are Bragg peaks in the columnar phase at $\mathbf{G} = (0, m_1 k_0/2, m_2 q_0)$ [denoted in the figure as (m_1, m_2) , where $m_1 + m_2$ is even]. In the columnar phase, DNA strands form a 2D lattice with true long-range order and associated x-ray Bragg peaks. In the sliding columnar and nematic lamellar phases, there are power-law quasi-Bragg peaks at $(2m_1, 0)$ and diffuse peaks at (m_1, m_2) for $m_1 \neq 0$. Dislocations destroy 2D smectic-like order in the nematic lamellar phase to produce more diffuse (m_1, m_2) peaks than in the sliding columnar phase. If interlayer couplings are weak and thermal fluctuations sufficiently strong, the $(\pm m, 1)$ peaks may merge to produce a diffuse peak centered at the rectangular-lattice $(0, 1)$ position in the sliding columnar and nematic lamellar phases. The labelling of peaks in this figure, which follows conventional (x, y, z) ordering for the our choice of axes, is the inverse of that of Ref. [4]. Thus (m_1, m_2) [e.g., $(\pm 1, 1)$] here corresponds to (m_2, m_1) [e.g., $(1, \pm 1)$] in Ref. [4].

Rather stringent conditions must be met before the SC phase can be thermodynamically stable. Thermal fluctuations must be strong enough to destroy the interlayer shear coupling present in the columnar phase but not so strong that dislocation proliferation destroys the smectic compressibility to create a nematic lamellar phase. The SC phase is stable only for temperatures T lying above a decoupling temperature T_d at which the C phase becomes unstable and below a KT-melting temperature T_{KT} above which the NL phase becomes stable. Thus a necessary condition for the SC phase to be stable is $T_d < T_{KT}$. In Sec. IV, we will show that this condition is violated for the nearest neighbor models we consider here. Elsewhere [13,14], we show that appropriately chosen interactions between further neighbor planes can stabilize the SC phase.

The focus of the paper is the rather unusual properties of the SC phase. We will, therefore, assume throughout most of the paper that the SC phase does exist. This approach is justified because it can under appropriate conditions be an equilibrium phase as discussed in Ref. [13] and because even if it is not thermodynamically stable, there is a range of length scales over which correlations functions will exhibit SC behavior.

This paper is composed of six sections, of which this is the first, and seven appendices, which mostly present mathematical details. Section II derives the Hamiltonians for the columnar, sliding columnar, and nematic lamellar phases, based on a model in which the dominant interactions are couplings between each DNA lattice and the two membranes on either side of it. Section III presents the correlation functions for the SC phase, in-

cluding x-ray scattering intensities. Section IV addresses the stability of the SC phase. It calculates T_d , and it derives general expressions for the interaction between dislocations before calculating T_{KT} . Section V presents a discussion of the various important length scales. Finally, Sec. VI provides an overview of results. Appendix A presents details of the derivation of the Hamiltonians in Sec. II. Appendices B through F provide details of the calculations of various SC phase correlations functions, and App. G presents details of calculations of interactions between dislocations.

II. MODEL FOR LAMELLAR PHASES OF DNA-LIPID COMPLEXES

A. Definition of Variables

As depicted in Fig. 1, lamellar phases of DNA-lipid complexes consist of a periodic stack of planar lipid bilayer membranes with spacing a separated by galleries intercalated with DNA strands that form a local 2D smectic lattice with preferred spacing d . Since our primary interest is in the nature of possible ordering of the DNA strands, we will assume that the lipid membranes are free of defects such as dislocations or focal conic structures that destroy their integrity. We can, therefore, specify a layer by its integer layer number n , and we can specify positions in the xz plane by the vector $\mathbf{r} = (x, z)$. We take the equilibrium height of the midpoint of bilayer membrane n be na . The height of membrane n at position \mathbf{r} is then

$$H_{\text{mem}}^n(\mathbf{r}) = na + h^n(\mathbf{r}), \quad (2.1)$$

where $h^n(\mathbf{r})$ is the Lagrangian height variable [15] measuring the displacement of layer n from its ideal height. The n th DNA lattice lies between membranes n and $n+1$. Its equilibrium height is, therefore, $(n + \frac{1}{2})a$, and its height at position \mathbf{r} is

$$H_{\text{DNA}}^n(\mathbf{r}) = (n + \frac{1}{2})a + u_y^n(\mathbf{r}), \quad (2.2)$$

where $u_y^n(\mathbf{r})$ measure deviations from equilibrium height.

The DNA lattice in layer n can be described in terms of a Fourier expansion of its density. It is important to keep track of the relative phases of mass-density waves in adjacent layers. In an ideal columnar lattice, the phase of the first mass-density wave in layer n is simply $q_0(z - z^n)$, where

$$q_0 = 2\pi/d \quad (2.3)$$

and z^n specifies the preferred position of lattices in different galleries. In a rectangular lattice, $z^n = 0$, and in a centered rectangular lattice, $z^n = nd/2$. Phase changes at position \mathbf{r} relative to the above ideal phases are produced by local translations described by the Eulerian displacement variable $u_z^n(\mathbf{r})$. Thus the DNA density-wave expansion in layer n is

$$\rho_{\text{DNA}}^n(\mathbf{r}) = \sum_k \rho^{nk}(\mathbf{r}) e^{ikq_0[z - z^n - u_z^n(\mathbf{r})]}. \quad (2.4)$$

If each DNA lattice is perfect with identical rods of linear density λ and separation d , then $\rho^{nk}(\mathbf{r}) = \lambda/d$ for every n and k . Thermal fluctuations will lead to reductions in ρ^{nk} that are larger for larger k . Thus, $\rho_{\text{DNA}}^n(\mathbf{x})$ can be approximated by

$$\rho_{\text{DNA}}^n(\mathbf{x}) \approx \rho_0 + \psi e^{iq_0[z - z^n - u_z^n(\mathbf{r})]} + \text{c.c.}, \quad (2.5)$$

where ψ , assumed to be independent of n , is the complex amplitude of the first non-trivial density wave.

The total mass density of DNA strands at positions $\mathbf{x} = (x, y, z) \equiv (\mathbf{r}, z)$ is

$$\rho_{\text{DNA}}(\mathbf{x}) = \sum_{nk} \rho^{nk}(\mathbf{r}) e^{ikq_0[z - z^n - u_z^n(\mathbf{r})]} \times f_{\text{DNA}}^k(y - (n + \frac{1}{2})a - u_y^n(\mathbf{r})), \quad (2.6)$$

where $f_{\text{DNA}}^k(y)$ is the form factor along the layer normal for a DNA mass-density wave of wavenumber kq_0 . If the DNA strands are lines with no width, the $f_{\text{DNA}}^k(y) = \delta(y)$. If the strands are modeled as cylinders of radius r_{DNA} , then the Fourier transform of $f_{\text{DNA}}^k(y)$ is [3]

$$f_{\text{DNA}}^k(q_y) = \frac{2J_1(\sqrt{q_y^2 + k^2q_0^2} r_{\text{DNA}})}{\sqrt{q_y^2 + k^2q_0^2} r_{\text{DNA}}}, \quad (2.7)$$

where $J_1(x)$ is the Bessel function of order 1. The membrane density is

$$\rho_{\text{mem}}(\mathbf{x}) = \sum_n \rho_L^0 f_{\text{mem}}[y - na - h^n(\mathbf{r})], \quad (2.8)$$

where ρ_L^0 is the area density of the lipid and $f_{\text{mem}}(y)$ is the lipid membrane form factor, which typically is equal to $1/w$ for $-w/2 < y < w/2$ where w is the membrane width. X-ray scattering experiments probe $\langle \rho(\mathbf{q})\rho(-\mathbf{q}) \rangle$, where $\rho(\mathbf{q})$ is the Fourier transform of a linear combination of $\rho_{\text{DNA}}(\mathbf{x})$ and $\rho_{\text{mem}}(\mathbf{x})$ [See Sec. III D].

B. Hamiltonian for Coupled DNA-Lipid Layers

We are now in a position to derive the Hamiltonian describing elastic fluctuations of lamellar DNA-lipid complexes. Our goal is to develop the simplest model consistent with symmetry. We begin with individual membranes and DNA layers. They are characterized by layer bending energies, which can be expressed as

$$\mathcal{H}^{\text{bend}} = \frac{1}{2} \sum_n a \int d^2r [K_{3d}[(\partial_x^2 + \partial_z^2)h^n]^2 + K_{2d}[(\partial_x^2 u_y^n)^2 + (\partial_x^2 u_z^n)^2]], \quad (2.9)$$

where $aK_{3d} = \kappa_{\text{mem}}$ is the bending rigidity of the lipid membranes and $adK_{2d} = \kappa_{\text{DNA}}$ is the bending rigidity of

an individual DNA strand. We adopt a convention here with a factor of the layer spacing a multiplying sums over n to facilitate the continuum limit: $\sum_n a \int d^2r \rightarrow \int d^3x$. Interactions between DNA strands lead to a preferred separation between strands within a layer and to a compressional elastic energy, characterized by a modulus B_{2d} , for changing this separation. There is also a preferred separation between a given DNA layer and the two lipid membranes above and below it. Harmonic deviations from this separation are characterized by a modulus B_{3d} . Changing the distance between membranes on either side of a DNA layer will lead to an expansion or a compression of its DNA smectic lattice, which is described by a coupling with strength B_{uh} between inplane strain and membrane separation. Combining all of these effects into a single compression energy, we obtain

$$\begin{aligned} \mathcal{H}^{\text{com}} = \sum_n a \int d^2r & \left[\frac{1}{2} B_{2d} (u_{zz}^n)^2 \right. \\ & + (B_{uh}/a) u_{zz}^n (h^{n+1} - h^n) \\ & \left. + (B_{3d}/a^2) [(h^{n+1} - u_y^n)^2 + (u_y^n - h^n)^2] \right], \end{aligned} \quad (2.10)$$

where

$$u_{zz}^n = \partial_z u_z^n - [(\partial_x u_z^n)^2 + (\partial_z u_z^n)^2]/2 \quad (2.11)$$

is the nonlinear 2D Eulerian strain and where factors of a^{-1} were introduced to facilitate the continuum limit, e.g., $(h^{n+1} - h^n)/a \sim \partial_y h(\mathbf{x})$. There are additional compressional energies involving interactions proportional to $(h^{n+1} - h^n)^2$, $(u_y^{n+1} - u_y^n)^2$, $(u_{zz}^{n+1} - u_{zz}^n)^2$, and other further neighbor terms. These are smaller than those considered in Eq. (2.10), and we will neglect them. They are, however, needed to achieve $T_d < T_{KT}$ and a stable SC phase [13].

Neighboring DNA strands within a gallery prefer to be parallel. This leads to a Frank-like orientational energy

$$\mathcal{H}^{\text{orien}} = \frac{1}{2} \sum_n a \int d^2r K_z (\partial_z \theta^n)^2, \quad (2.12)$$

where $\theta^n(\mathbf{r}) \approx \partial_x u_z^n(\mathbf{r})$ is the angle that the n th DNA lattice at \mathbf{r} makes with the x -axis. In all but the NL phase, this orientational interaction is subdominant to those in Eq. (2.9), and we will ignore it.

Finally, there are interactions between DNA lattices in neighboring galleries that favor parallel alignment and spatial registry of the lattices. These interactions are described by a sum of layer-coupling Hamiltonians

$$\mathcal{H}^{\text{int}} = \sum_n (\mathcal{H}_n^\theta + \mathcal{H}_n^u). \quad (2.13)$$

The angular coupling is

$$\mathcal{H}_n^\theta = -V^\theta \int d^2r \cos[2(\theta^n - \theta^{n+1})]. \quad (2.14)$$

In all but the isotropic lamellar phase, there is long-range angular order, and we can replace $\sum_n \mathcal{H}_n^\theta$ by

$$\mathcal{H}^{\text{rot}} = \frac{1}{2} K_y \sum_n a \int d^2r \left(\frac{\partial_x u_z^{n+1} - \partial_x u_z^n}{a} \right)^2, \quad (2.15)$$

where $K_y \approx 4aV^\theta e^{-4((\theta^n)^2)}$. The interaction \mathcal{H}_n^u in Eq. (2.13), favoring spatial registry, arises from interactions between DNA densities in Eq. (2.5). The phases $q_0 z^n$ [Eq. (2.4)] are chosen so that energy is minimized when the remaining phase, $\beta^n(\mathbf{r}) = q_0[z - u_z^n(\mathbf{r})]$, of mass-density waves in neighboring DNA lattices are equal at the points of closest approach of the lattices [Fig. 3]. The point at \mathbf{r}^{n+1} in layer $n+1$ closest to the point at \mathbf{r}^n in layer n lies along the normal $\mathbf{N}^n(\mathbf{r}) \approx (-\partial_x u_y^n, 1, -\partial_z u_y^n)$. Thus $\mathbf{r}^{n+1} = \mathbf{r}^n + \delta\mathbf{r}^{n+1}$, where $\delta\mathbf{r}^{n+1} = a\mathbf{N}_\perp \approx (-a\partial_x u_y^n, 0, -a\partial_z u_y^n)$ where \mathbf{N}_\perp is the projection of \mathbf{N} onto the xz plane. Energy is minimized when $\beta^{n+1}(\mathbf{r}^{n+1}) = q_0(z - a\partial_z u_y^n - u_z^{n+1})$ is equal to $\beta^n(\mathbf{r}^n)$. The resulting energy is

$$\mathcal{H}_n^u = -V^u \int d^2r \cos[q_0(u_z^{n+1} - u_z^n + a\partial_z u_y^n)], \quad (2.16)$$

where V^u is proportional to the square $|\psi|^2$ of the mass-density-wave amplitude. As required, this energy is invariant with respect to spatially uniform translations described by an n - and \mathbf{r} -independent displacement of $u_z^n(\mathbf{r})$. It is also invariant to harmonic order with respect to uniform rotations in which $u_z^{n+1} - u_z^n = -a\partial_z u_y^n$. The predominant interaction between DNA in neighboring strands is electrostatic, and we expect $V^u \sim (\lambda_e^2/d)e^{-2\pi a/d}$, where λ_e is the charge per unit length on a DNA strand.

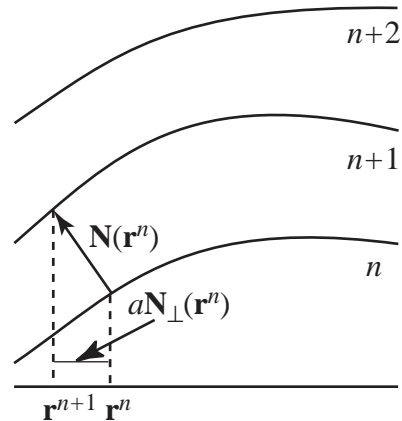


FIG. 3. A sequence of tilted and bent membranes. Interactions favor equality of the shifted phase, $\beta^n(\mathbf{r}) = q_0[z - u_n(\mathbf{r})]$, in neighboring layers at points of closest approach, i.e., they favor $\beta^n(\mathbf{r}^n) = \beta^{n+1}(\mathbf{r}^{n+1})$ where $\mathbf{r}^{n+1} - \mathbf{r}^n = a\mathbf{N}_\perp(\mathbf{r}^n)$, where \mathbf{N}_\perp is the projection of the membrane layer normal onto the yz plane.

To summarize, our complete model Hamiltonian coupling membrane height displacements h^n and DNA lattice displacements u_y^n and u_z^n is thus

$$\mathcal{H}^{\text{tot}} = \mathcal{H}^{\text{bend}} + \mathcal{H}^{\text{com}} + \mathcal{H}^{\text{int}}, \quad (2.17)$$

with entries defined by Eqs. (2.9), (2.10), and (2.13) to (2.16).

1. Effective Hamiltonian for DNA Displacements

Though we will discuss membrane height fluctuations, our primary focus will be on properties of the DNA lattices. It is, therefore, useful to integrate out the membrane height variables $h^n(\mathbf{r})$ to obtain an effective Hamiltonian for DNA displacements only. This operation is carried out in Appendix A. The long wavelength result is

$$\mathcal{H}_{DNA}^{\text{tot}} = \mathcal{H}^{SC} + \mathcal{H}^u \quad (2.18)$$

where $\mathcal{H}^u = \sum_n \mathcal{H}_n^u$ and \mathcal{H}^{SC} is the sliding phase Hamiltonian,

$$\begin{aligned} \mathcal{H}^{SC} = & \frac{1}{2} \sum_n a \int d^2r [B_{2d}(u_{zz}^n)^2 + K_{2d}(\partial_x^2 u_z^n)^2] \\ & + \frac{1}{2} \sum_n a \int d^2r [(B_{3d}/a^2)(u_y^{n+1} - u_y^n)^2 + K^{\alpha\beta}(\partial_\alpha \partial_\beta u_y^n)^2] \\ & + \frac{1}{2} \sum_n a \int d^2r [-B_{zz}[(u_{zz}^{n+1} - u_{zz}^n)/a]^2 \\ & \quad + 2(B_{uh}/a)u_{zz}^n(u_y^{n+1} - u_y^{n-1})] \\ & - \frac{1}{2} \sum_n a \int d^2r K_y[(\partial_x u_z^{n+1} - \partial_x u_z^n)/a]^2 \end{aligned} \quad (2.19)$$

where

$$B_{zz} = \frac{B_{uh}^2}{4B_{3d}}, \quad (2.20)$$

the summation convention on $\alpha = x, z$ and $\beta = x, z$ is understood, and the bending-rigidity tensor is

$$K^{\alpha\beta} = \begin{pmatrix} K^{xx} & K^{xz} \\ K^{zx} & K^{zz} \end{pmatrix} = \begin{pmatrix} K_{3d} + K_{2d} & K_{3d} \\ K_{3d} & K_{3d} \end{pmatrix}. \quad (2.21)$$

Note that integrating out h^n creates interactions between nearest-neighbor and next-nearest-neighbor u_z^n and u_y^n displacements not present in the original model of Eq. (2.17). These interactions, however, have particular ratios determined by the parameters in \mathcal{H}^{tot} . Of particular importance to us in what follows is the fixed relations between the coefficients of $(u_y^{n+1} - u_y^n)^2$, $(u_{zz}^{n+1} - u_{zz}^n)^2$, and $u_{zz}^n(u_y^{n+1} - u_y^{n-1})$. In a more general model with further-neighbor interactions, the simple relation of Eq. (2.20) among B_{zz} , B_{uh} , and B_{3d} would not hold.

Using $\mathcal{H}_{DNA}^{\text{tot}}$, we can construct the long-wavelength Hamiltonian for each of the phases listed in the introduction as detailed in the following.

2. The Columnar Phase

The columnar crystal is characterized by strong coupling of displacements in different layers. Its elastic Hamiltonian can be obtained by expanding the cosine in \mathcal{H}_n^u [Eq. (2.16)] about one of its minima. Performing this operation, taking the continuum limit, and retaining only the lowest order terms in a gradient expansion, we obtain the familiar elastic Hamiltonian for a rectangular columnar lattice [16]:

$$\begin{aligned} \mathcal{H}^C = & \frac{1}{2} \int d^3x [B_{2d}u_{zz}^2 + B_{3d}u_{yy}^2 + B_{uh}u_{zz}u_{yy} + B_{yz}u_{yz}^2] \\ & + \int d^3x [K_{2d}(\partial_x^2 u_z)^2 + (K_{2d} + K_{3d})(\partial_x^2 u_y)^2] \end{aligned} \quad (2.22)$$

where $\mathbf{x} = (\mathbf{r}, na)$, $u_{zz}(\mathbf{x}) = u_{zz}^{n=y/a}(\mathbf{r})$, and $B_{yz} \approx V^u q_0^2 a^2$. Note that the shear elastic modulus B_{yz} arises from \mathcal{H}_n^u and is zero when V^u is zero. The cross compression B_{uh} -term arises from the $u_{zz}^n(u_y^{n+1} - u_y^n)$ term in $\mathcal{H}_{DNA}^{\text{tot}}$, which was generated by the interaction of u_{zz}^n with the membrane height field h^n

3. Sliding Columnar Phase

The sliding columnar phase is characterized by a vanishing shear modulus B_{yz} for relative displacement of DNA lattices. Its dominant fluctuations are, therefore, described by the Hamiltonian \mathcal{H}^{SC} of Eq. (2.19) obtained by setting $V^u = 0$ in $\mathcal{H}_{DNA}^{\text{tot}}$. The V^u coupling is irrelevant when the sliding phase is stable as detailed in the following [See Sec. IV].

4. Nematic Lamellar Phase

Positional couplings between layers and the smectic compression modulus B_{2d} both vanish in the nematic lamellar phase, and

$$\begin{aligned} \mathcal{H}^{\text{NL}} = & \frac{1}{2} \int d^3x [K_x(\partial_x \theta)^2 + K_y(\partial_y \theta)^2 + K_z(\partial_z \theta)^2] \\ & + \frac{1}{2} \int d^3x [B_{3d}u_{yy}^2 + K^{\alpha\beta}(\partial_\alpha \partial_\alpha u_y)^2]. \end{aligned} \quad (2.23)$$

where $K_x = K_{2d}$ and K_z is a Frank elastic constant introduced in Eq. (2.12).

III. CORRELATIONS IN THE SLIDING COLUMNAR PHASE

In the preceding section, we derived a general Hamiltonian capable of describing the phases of lamellar DNA-lipid complexes. In this section, we will investigate correlations in the sliding columnar phase. The most unusual

correlations in the sliding columnar phase are those involving displacements of DNA strands within the layers. We will thus begin by considering the effective Hamiltonian for u_z^n obtained by integrating out u_y^n from \mathcal{H}^{SC} [Eq. (2.19)]. From this we will calculate all correlation functions of u_z^n . We will then consider membrane height correlations described by an effective Hamiltonian for h^n in which u_y^n and u_z^n have been integrated out of \mathcal{H}^{tot} [Eq. (2.17)]. In the long-wavelength limit fluctuations in u_y^n are the same as those in h^n . Finally, we will discuss the relevancy of the shear coupling V^u , Eq. (2.16). This involves a consideration of both u_z^n and $\partial_z u_y^n$.

A. Correlations in u_z^n

1. Effective Hamiltonian for u_z^n

Since u_y^n and u_z^n are harmonically coupled in $\mathcal{H}_{DNA}^{\text{tot}}$, we can integrate over u_y^n exactly to obtain an effective Hamiltonian for u_z^n fluctuations alone. This calculation is carried out in Appendix A. In the long-wavelength limit, the resulting Hamiltonian is

$$\mathcal{H}_z^{SC} = \frac{1}{2} \sum_n a \int d^2r \left[B(u_{zz}^n)^2 + K(\partial_x^2 u_z^n)^2 \right] \quad (3.1a)$$

$$+ \frac{K_y}{a^2} [\partial_x(u_z^n - u_z^{n+1})]^2 \quad (3.1b)$$

where $K = K_{2d}$ and

$$B = B_{2d} - (B_{uh}^2/B_{3d}). \quad (3.2)$$

Note that there is no term proportional to $(u_{zz}^{n+1} - u_{zz}^n)^2$ in Hamiltonian \mathcal{H}_z^{SC} even though there is one in \mathcal{H}^{SC} . This is a result of the special relation [Eq. (2.20)] among energy coefficients in \mathcal{H}^{SC} .

The Hamiltonian of Eq. (3.1) is the sum of two parts: a sum of elastic energies for independent $2D$ smectics [Eq. (3.1a)] and a term coupling angles in neighboring layers [Eq. (3.1b)]. The $2D$ smectic energy is a function of the full nonlinear strain u_{zz}^n . When $K_y = 0$ and there is no coupling between layers, nonlinearities in u_{zz}^n lead to important renormalizations of the long-wavelength elastic constant of a $2D$ smectic [10]. When the interlayer coupling term is present, nonlinearities in u_{zz}^n also lead to long wavelength renormalization of elastic constants in the SC phase [17]. These renormalizations are only logarithmic, however, and we will ignore them in this article.

We, therefore, consider the harmonic limit of \mathcal{H}_z^{SC} , which is conveniently expressed in Fourier space. Introducing

$$\int \frac{d^3q}{(2\pi)^2} = \int_{-\pi/a}^{\pi/a} \frac{dq_y}{2\pi} \int_{-\Lambda_x}^{\Lambda_x} \frac{dq_x}{2\pi} \int_{-\Lambda_z}^{\Lambda_z} \frac{dq_z}{2\pi} \quad (3.3)$$

where Λ_x and $\Lambda_z \sim 2\pi/d$ are wavenumber cutoffs, and

$$u_z^n(\mathbf{r}) = \int \frac{d^3q}{(2\pi)^3} e^{i(q_y n a + \mathbf{q}_\perp \cdot \mathbf{r})} u_z(\mathbf{q}), \quad (3.4)$$

where $\mathbf{q}_\perp = (q_x, 0, q_z)$, we obtain

$$\mathcal{H}_z^{SC} = \frac{1}{2} \int \frac{d^3q}{(2\pi)^3} [Bq_z^2 + Kq_x^4 + K_y(q_y)q_x^2q_y^2] |u_z(\mathbf{q})|^2. \quad (3.5)$$

Here

$$K_y(q_y) = K_y p(q_y a) \quad (3.6)$$

with

$$p(q_y a) = 2 \frac{(1 - \cos q_y a)}{(q_y a)^2}, \quad (3.7)$$

which tends to unity as $q_y a \rightarrow 0$ so that $K(q_y = 0) = K_y$.

Two important length scales can be obtained from Eq. (3.1) by comparing the orientational interaction energy with the $2D$ smectic compression and bending energies. The lengthscales

$$x^* = \frac{a}{\mu_y} \quad \text{and} \quad z^* = \frac{a^2}{\mu_y^2 \lambda}, \quad (3.8)$$

with $\mu_y = \sqrt{K_y/K}$ and $\lambda = \sqrt{K/B}$, separate two-dimensional from three-dimensional behavior. At lengthscales within a gallery less than x^* and z^* , the $2D$ compression and bending energies are large compared to the orientational interaction, and the DNA lattices behave like independent $2D$ smectics. On the other hand, at lengthscales greater than x^* and z^* , the orientational interaction is significant, and $3D$ sliding behavior occurs.

Before proceeding to discuss the sliding phase correlations, we note that the sliding phase elastic free energy in Eq. (3.1) exhibits a striking *local* (gauge) translational invariance of the form

$$u_z(x, z, na) \rightarrow u_z(x, z, na) + f(n); \quad (3.9)$$

here the displacement $f(n)$ is an *arbitrary* function of n assuming a different value in each gallery. In other words, the DNA lattices in different galleries can continuously slide relative to each other by arbitrary distances with no elastic energy costs. In a standard columnar phase, this continuous symmetry is spontaneously broken down by the shear coupling in Eq. (2.16). On the other side, in the sliding phase, this shear coupling is irrelevant at long scales, and elastic properties reflect the gauge symmetry in Eq. (3.1). This symmetry is entirely responsible for the unconventional fluctuation behavior of the sliding phase we discuss in the following. In particular, we find that in the sliding phase, the fluctuations of relative displacements $u_z^{n+1}(\mathbf{r}) - u_z^n(\mathbf{r})$ of DNA lattices in neighboring galleries diverge in thermodynamic limit. As a reflection of the gauge symmetry Eq. (3.1), a DNA lattice in a gallery is essentially free to flow relative to DNA lattices in neighboring galleries. The sliding phase thus exhibits zero macroscopic shear modulus [6,7]

2. Definitions of Correlation Functions

Correlations in u_z^n follow directly from Eq. (3.5):

$$\begin{aligned} G_{zz}(\mathbf{r}, na) &= \langle u_z^n(\mathbf{r}) u_z^0(0) \rangle \equiv \langle (u_z^n(\mathbf{r}))^2 \rangle - g(\mathbf{r}, na) \\ &= \int \frac{d^3q}{(2\pi)^3} G_{zz}(\mathbf{q}) e^{i(\mathbf{q}_\perp \cdot \mathbf{r} + q_y na)}, \end{aligned} \quad (3.10)$$

where

$$G_{zz}(\mathbf{q}) = \frac{T}{Bq_z^2 + Kq_x^4 + K_y q_x^2 q_y^2 p(q_y a)}, \quad (3.11)$$

$$\langle (u_z^n)^2 \rangle = \int \frac{d^3q}{(2\pi)^3} G_{zz}(\mathbf{q}), \quad (3.12)$$

and

$$\begin{aligned} g(\mathbf{r}, na) &= \frac{1}{2} \langle [u_z^n(\mathbf{r}) - u_z^0(\mathbf{0})]^2 \rangle \\ &= \int \frac{d^3q}{(2\pi)^3} G_{zz}(\mathbf{q}) \left[1 - e^{i(\mathbf{q}_\perp \cdot \mathbf{r} + q_y na)} \right]. \end{aligned} \quad (3.13)$$

It is useful to decompose $g(\mathbf{r}, na)$ into three parts:

$$g(\mathbf{r}, na) = g^{(1)}(na) + g^{(2)}(\mathbf{r}) - g^{(3)}(\mathbf{r}, na), \quad (3.14)$$

where

$$\begin{aligned} g^{(1)}(na) &= \frac{1}{2} \langle [u_z^n(\mathbf{0}) - u_z^0(\mathbf{0})]^2 \rangle \\ &= \int \frac{d^3q}{(2\pi)^3} G_{zz}(\mathbf{q}) (1 - \cos q_y na) \end{aligned} \quad (3.15)$$

$$\begin{aligned} g^{(2)}(\mathbf{r}) &= \frac{1}{2} \langle [u_z^0(\mathbf{r}) - u_z^0(\mathbf{0})]^2 \rangle \\ &= \int \frac{d^3q}{(2\pi)^3} G_{zz}(\mathbf{q}) (1 - e^{i\mathbf{q}_\perp \cdot \mathbf{r}}) \end{aligned} \quad (3.16)$$

$$\begin{aligned} g^{(3)}(\mathbf{r}, na) &= -\langle [u_z^n(\mathbf{0}) - u_z^0(\mathbf{0})][u_z^n(\mathbf{r}) - u_z^0(\mathbf{0})] \rangle \\ &= \int \frac{d^3q}{(2\pi)^3} G_{zz}(\mathbf{q}) \\ &\quad \times (1 - \cos q_y na)(1 - e^{i\mathbf{q}_\perp \cdot \mathbf{r}}). \end{aligned} \quad (3.17)$$

It is clear that $g^{(1)}(na) = g(0, na)$ and $g^{(2)}(\mathbf{r}) = g(\mathbf{r}, 0)$. Each of these functions has a characteristic singular behavior as a function of system size and separation, which we will summarize below. Finally, the function

$$g^{(2)}(\mathbf{r}, na) = g^{(2)}(\mathbf{r}) - g^{(3)}(\mathbf{r}, na) \quad (3.18)$$

will appear in our derivation in App. F of interplane density correlations discussed in Sec. III D.

3. Asymptotic Forms for $K_y \neq 0$

The local fluctuation $\langle (u_z^n)^2 \rangle$ in the SC phase diverges as the *square* of the log of the system size with a functional form that depends on the order in which the sample dimensions L_x , L_y , and L_z along the x , y and z directions approach infinity:

$$\langle (u_z^n)^2 \rangle = l_u^2 \begin{cases} \ln^2 [8L_x/x^*] & L_z \gg L_y \sim L_x \\ \frac{1}{2} \ln^2 [\alpha_z L_z/z^*] & L_x \gg L_y \sim L_z \end{cases}, \quad (3.19)$$

where the length l_u is defined via

$$l_u^2 = \frac{T}{4\pi^2 \sqrt{BK_y}}, \quad (3.20)$$

α_z is a number, $L_z \gg z^*$, $L_x \gg x^*$, and terms that do not diverge with system size have been dropped. The calculation of the displacement fluctuations in the limit $L_z \rightarrow \infty$ and $L_x \sim L_y$ is detailed in Appendix B. Thus, SC “in-plane” fluctuations are less divergent than 2D smectic fluctuations that scale as a power-law with system size but more divergent than 3D Landau-Peierls smectic lamellar fluctuations that grow logarithmically with system size [9,10]. The mean-square angular fluctuation, $\langle (\theta^n)^2 \rangle = \langle (\partial_x u_z^n)^2 \rangle$, is finite, implying that the SC phase has three-dimensional long-range orientational order.

The $\ln^2 L_{x,z}$ divergence of $\langle (u_z^n)^2 \rangle$ is converted to a $\ln^2 r$ divergence in the function $g^{(2)}(\mathbf{r})$ [Eq. (3.16)]. In Appendix D, we outline the calculation of $g^{(2)}(\mathbf{r})$ for large r . The results [6,7] are

$$g^{(2)}(\mathbf{r}) = l_u^2 \begin{cases} \ln^2 [8e^\gamma x/x^*] + C_x & \text{if } z = 0 \\ \frac{1}{2} \ln^2 [32e^\gamma z/z^*] + C_z & \text{if } x = 0, \end{cases} \quad (3.21)$$

where $\gamma \approx 0.577$ is Euler’s constant and C_x and C_z are constants that depend on Λ_x and Λ_z but have well-defined $\Lambda_{x,z} \rightarrow \infty$ limits. Note that the only $\Lambda_{x,z}$ dependence of the correlation function in these two large distance limits is found in the constants C_x and C_z . C_x and C_z are evaluated in Appendix D in the continuum limit ($\Lambda_{x,z} \rightarrow \infty$) in which we find $C_x = 0$ and $C_z = \pi^2/8$.

The function $g^{(1)}(na)$ [Eq. (3.15)] is by definition zero when $n = 0$. For all $n \neq 0$, it diverges logarithmically with system size:

$$g^{(1)}(na) = 2l_u^2 S_n(0) \ln \left[A_n(\Lambda_x, \Lambda_z) \frac{L_x}{x^*} \right], \quad (3.22)$$

where

$$S_n(t) = \int_0^\pi du \frac{1 - \cos(nu)}{\sqrt{t^2 + u^2 p(u)}}, \quad (3.23)$$

$$S_n(0) = \sum_{k=1}^n \frac{2}{2k-1}, \quad (3.24)$$

and $A_n(\Lambda_x, \Lambda_z)$ calculated in App. C depends on the layer separation n and the ultraviolet cutoffs but has a well-defined $\Lambda_{x,z} \rightarrow \infty$ limit that is calculated in Appendix C.

The function $g^{(3)}(\mathbf{r}, na)$ [Eq. (3.17)] is also zero at $n = 0$. It has the same divergences as a function of separation r that $g^{(1)}(na)$ has with system size:

$$g^{(3)}(\mathbf{r}, n) = 2l_u^2 S_n(0) \begin{cases} \ln(D_n x/x^*) & \text{if } z = 0 \\ \ln(E_n a z/z^*) & \text{if } x = 0. \end{cases} \quad (3.25)$$

where D_n and E_n are numerical constants that have well defined values in the continuum limit, $\Lambda_x, \Lambda_z \rightarrow \infty$, as discussed in App. E.

It is useful to summarize the results of the calculations just presented. When $n = 0$, i.e., for points in the same layer, $g(\mathbf{r}, 0) = g^{(2)}(\mathbf{r})$ grows with r as $\ln^2 r$. When $n \neq 0$, i.e., for sites in different layers, $g(\mathbf{r}, na)$ diverges logarithmically with system size for all \mathbf{r} because $g^{(1)}(na)$ diverges in this way. If $g^{(1)}(na)$ is subtracted from $g(\mathbf{r}, n)$, then the remaining function, $g^{(2)}(\mathbf{r}, na)$, grows with r as $\ln^2(r/r_n)$ with r_n depending on the coefficient of $\ln r$ in $g^{(3)}(\mathbf{r}, na)$ when $n \neq 0$.

4. The limit $K_y = 0$: 2D Smectic Correlations

When $K_y = 0$, there are no interactions between planes (when $V^u = 0$), and the system reduces to a stack of independent 2D smectic planes. Since experiments [3] are consistent with nearly independent 2D smectic layers, we will review here well established results [10] for such systems.

Decoupled smectics are described by the Hamiltonian of Eq. (3.1a) obtained by setting $K_y = 0$ in \mathcal{H}^{SC} . This Hamiltonian is a function of the full nonlinear 2D strain u_{zz}^n . Nonlinearities lead to important deviations from harmonic behavior. Since there is no coupling between layers, $G_{zz}(\mathbf{q})$ is independent of q_y , and we can define a 2D correlation function $G_2(\mathbf{q}_\perp) = G_{zz}(\mathbf{q})/a$.

At lengthscales less than the nonlinear lengths

$$l_x = \frac{8\pi K_2^{3/2}}{T\sqrt{B_2}} \quad \text{and} \quad l_z = \frac{l_x^2}{\lambda}, \quad (3.26)$$

where $K_2 = Ka$ and $B_2 = Ba$ are 2D bend and compression moduli and $\lambda = \sqrt{K_2/B_2}$, nonlinearities are unimportant, and 2D smectic fluctuations are described by the linearized elastic Hamiltonian \mathcal{H}_z^{SC} of Eq. (3.5) with $K_y = 0$ [10]. At lengthscales longer than l_x and l_z , the nonlinear terms in the rotationally invariant strain in Eq. (2.11) lead to renormalized bending and compression moduli $K_2(\mathbf{q}_\perp)$ and $B_2(\mathbf{q}_\perp)$ that, respectively, diverge and vanish at small wavenumber \mathbf{q}_\perp [10]. Note that the nonlinear lengths l_x and l_z decrease with increasing temperature, and thus nonlinearities become important at high temperatures. In both the harmonic and nonlinear regimes, the Fourier transformed displacement correlation function $\langle |u_z^n(\mathbf{q})|^2 \rangle$ in each gallery were expressed as

$$G_2(\mathbf{q}_\perp) = \frac{T}{B_2(\mathbf{q}_\perp)q_z^2 + K_2(\mathbf{q}_\perp)q_x^4} = \frac{T}{B_2} l_z^2 \tilde{q}_x^{-\gamma} Q(\tilde{q}_z/\tilde{q}_x^\nu), \quad (3.27)$$

where $\tilde{q}_{x,z} = q_{x,z} l_{x,z}$ and

$$\tilde{q}_x^{-\gamma} Q(\tilde{q}_z/\tilde{q}_x^\nu) \sim \begin{cases} \tilde{q}_x^{-\gamma}, & \tilde{q}_z = 0 \\ \tilde{q}_z^{-\gamma/\nu}, & \tilde{q}_x = 0. \end{cases} \quad (3.28)$$

The scaling form of the correlation function implies that $K_2(q_x, q_z = 0) \sim q_x^{-4+\gamma}$ and $B_2(q_x = 0, q_z) \sim q_z^{-2+\gamma/\nu}$. In the harmonic regime where $q_{x,z} l_{x,z} > 1$, $K_2(\mathbf{q}_\perp) = K_2$ and $B_2(\mathbf{q}_\perp) = B_2$ are constants, and the scaling exponents are $\gamma = 4$ and $\nu = 2$. In the anharmonic regime $q_{x,z} l_{x,z} < 1$, the scaling exponents γ and ν were calculated exactly by mapping the 2D smectic model with thermal fluctuations onto the KPZ model in 1+1 dimensions [10]. The exponents in the anharmonic regime are $\gamma = 7/2$ and $\nu = 3/2$.

The mean-square displacement fluctuations diverge in both regimes with lengths L_x and L_z of the sample in the xz plane:

$$\langle u_z^2(\mathbf{r}) \rangle = \int \frac{d^2 q_\perp}{(2\pi)^2} G_2(\mathbf{q}_\perp) = \lambda^2 \tilde{L}_x^{2\alpha} f_u^{(1)}(\tilde{L}_z/\tilde{L}_x^\nu), \quad (3.29)$$

where $u_z(\mathbf{r}) \equiv u_z^n(\mathbf{r})$, $2\alpha = \gamma - 1 - \nu = 1$ in both regimes, $\tilde{L}_{x,z} = L_{x,z}/l_{x,z}$, $f_u^{(1)}(0) = \text{const.}$, and $f_u^{(1)}(w) \sim w^{2\alpha/\nu}$ as $w \rightarrow \infty$. This implies that the Debye-Waller factor $\langle \exp[iq_0 u_z] \rangle^2 = \exp[-q_0^2 \langle u_z^2 \rangle] = 0$ in the limit of infinite system size, and there is no long-range positional order at any finite temperature in a 2D smectic, even when there are no dislocations.

Since the mean-square displacement fluctuations diverge as a power-law with system size, the displacement correlation function

$$g^{2D}(\mathbf{r}) = \frac{1}{2} \langle [u_z^n(\mathbf{r}) - u_z^n(0)]^2 \rangle = \lambda^2 |\tilde{x}|^{2\alpha} f_u^{(2)}(|\tilde{z}|/|\tilde{x}|^\nu) \quad (3.30)$$

diverges algebraically with in-plane separation r . In Eq. (3.30), $\tilde{x} = x/l_x$, $\tilde{z} = z/l_z$, and the scaling behavior of $f_u^{(2)}(w)$ is similar to that of $f_u^{(1)}(w)$. In the harmonic limit,

$$q_0^2 g^{2D}(\mathbf{r}) = \begin{cases} (z/\xi_x)^{1/2}, & \text{if } x = 0; \\ (x/\xi_x), & \text{if } z = 0, \end{cases} \quad (3.31)$$

where

$$\xi_z = \frac{\lambda B_2^2 d^4}{4\pi^3 T^2} \quad (3.32)$$

is correlation length along z and $\xi_x = \lambda(d/\pi)^2(B_2/T) = 2\sqrt{\lambda\xi_z/\pi}$ is a correlation length along x . These correlation lengths are measured in x-ray scattering experiments at sufficiently short length scales when layers are decoupled.

Fluctuations in the angle $\theta = \partial_x u_z$ are nondivergent because of an additional factor of q_x^2 in the numerator of (3.29). Finite angular fluctuations imply that $\langle \cos \theta \rangle = \exp[-\langle \theta^2 \rangle/2]$ is nonzero, and thus there is long-range orientational order in 2D smectics when there are no dislocations [9].

B. Correlations in $h^n(\mathbf{r})$ and $u_y^n(\mathbf{r})$.

In the absence of order in the DNA strands, lamellar DNA lipid complexes are simply multicomponent isotropic lamellar systems with height fluctuations identical to those of any isotropic lamellar smectic. The presence of orientational order in the DNA lattices introduces anisotropy into the effective bending moduli of the lipid membranes. By integrating out $u_y^n(\mathbf{r})$ and $u_z^n(\mathbf{r})$ from the complete Hamiltonian \mathcal{H}^{tot} of Eq. (2.17), we obtain in App. A an effective Hamiltonian for height fluctuations. In the long-wavelength limit, this effective Hamiltonian is

$$\mathcal{H}_h^{SC} = \frac{1}{2} \sum_n a \int d^2r \left[(B_{\text{lam}}/a^2)(h^{n+1} - h^n)^2 + K^{\alpha\beta} (\partial_\alpha \partial_\beta h^n)^2 \right], \quad (3.33)$$

where

$$B_{\text{lam}} = B_{3d} - (B_{uh}^2/B_{2d}) \quad (3.34)$$

and $K^{\alpha\beta}$ is the bending-rigidity tensor defined in Eq. (2.21). The model in Eq. (3.33) is an anisotropic version of the discrete smectic Hamiltonian often used to describe lamellar systems [18,19]. An effective Hamiltonian for DNA-lattice height displacements $u_y^n(\mathbf{r})$ can be obtained by integrating over $h^n(\mathbf{r})$ and $u_z^n(\mathbf{r})$ in \mathcal{H}^{tot} of Eq. (2.17). The resulting Hamiltonian is identical in the long-wavelength limit to \mathcal{H}_h in Eq. (3.33). Thus correlations in $u_y(\mathbf{r})$ are identical in this model in the long-wavelength limit to those in $h^n(\mathbf{r})$.

Fluctuations in h^n are determined by the correlation function

$$G_{hh}(\mathbf{q}) = \frac{T}{B_{\text{lam}} q_y^2 p(q_y a) + K^{\alpha\beta} q_\alpha^2 q_\beta^2}, \quad (3.35)$$

where $K^{\alpha\beta} q_\alpha^2 q_\beta^2 = K_{3d}(q_x^2 + q_z^2)^2 + K_{2d} q_x^4$. This equation implies that $\langle [h^n(\mathbf{r})]^2 \rangle$ diverges logarithmically with system size as it does in ordinary isotropic lamellar systems. The coefficient of the system-size logarithm depends on the anisotropy in $K^{\alpha\beta}$. Similarly, correlations in $h^n(\mathbf{r})$ defined via

$$\begin{aligned} g_h(\mathbf{r}, na) &= \frac{1}{2} \langle [h^n(\mathbf{r}) - h^0(\mathbf{0})]^2 \rangle \\ &= \frac{1}{2} \langle [u_y^n(\mathbf{r}) - u_y^0(\mathbf{0})]^2 \rangle \\ &= \int \frac{d^3q}{(2\pi)^3} G_{hh}(\mathbf{q}) [1 - e^{i(\mathbf{q}_\perp \cdot \mathbf{r} + q_y na)}] \end{aligned} \quad (3.36)$$

diverge logarithmically with na and \mathbf{r} :

$$k_0^2 g_h(\mathbf{r}, na) = \begin{cases} \eta_h \ln(na \lambda_x \Lambda^2) & \text{if } \mathbf{r} = \mathbf{0} \\ 2\eta_h \ln(\tilde{\Lambda}(\theta)r) & \text{if } n \neq 0, \end{cases} \quad (3.37)$$

where $\lambda_x = \sqrt{B/K^{xx}}$, $k_0 = 2\pi/a$, and

$$\eta_h = \frac{k_0^2 T}{8\pi^2 \sqrt{B_{\text{lam}} K^{xx}}} I(K^{xz}/K^{xx}, K^{zz}/K^{xx}), \quad (3.38)$$

where

$$I(\mu, \nu) = \frac{1}{2\pi} \int_{-\pi}^{\pi} \frac{d\theta}{\sqrt{\cos^4 \theta + 2\mu \sin^2 \theta \cos^2 \theta + \nu \sin^4 \theta}}. \quad (3.39)$$

In Eq. (3.37), Λ and $\tilde{\Lambda}(\theta)$ are cutoffs that depend on Λ_x , Λ_z and ratios of bending moduli. In addition, $\tilde{\Lambda}(\theta)$ depends on the angle θ that \mathbf{r} makes with the x axis.

C. Density Correlations

The DNA density correlation function arising from displacements parallel to lipid membranes is

$$S(\mathbf{r}, na) = \langle \exp(iq_0[u_z^n(\mathbf{r}) - u_z^0(\mathbf{0})]) \rangle. \quad (3.40)$$

This function is easily evaluated in the SC phase when $V^u = 0$:

$$S(\mathbf{r}, na) = e^{-q_0^2 g(\mathbf{r}, na)}, \quad (3.41)$$

where $g(\mathbf{r}, na)$ is the displacement correlation function defined in Eq. (3.13). Since $g(\mathbf{r}, na)$ diverges with the system size for all $n \neq 0$, $S(\mathbf{r}, na)$ vanishes in the thermodynamic limit for all $n \neq 0$. Thus, DNA densities in different layers are completely uncorrelated in the SC phase when the coupling V^u in Eq. (2.16) is set to zero.

1. In-plane Correlations

When $n = 0$, $g(\mathbf{r}, na)$ does not diverge in the thermodynamic limit, and we have

$$S_2(\mathbf{r}) \equiv S(\mathbf{r}, 0) = \langle e^{iq_0[u_z^n(\mathbf{r}) - u_z^n(0)]} \rangle = e^{-q_0^2 g^{(2)}(\mathbf{r})}, \quad (3.42)$$

with $g^{(2)}(\mathbf{r})$ given by Eq. (3.16). Thus, from Eqs. (3.21) and (3.30),

$$S_2(x, 0) = \begin{cases} S_x e^{-q_0^2 t_u^2 \ln^2[8e^\gamma x/x^*]}, & x \gg x^*; \\ e^{-q_0^2 g^{2D}(x, 0)}, & x \ll x^*, \end{cases} \quad (3.43)$$

where $S_x = e^{-q_0^2 t_u^2 C_x}$ is a constant, and $g^{2D}(\mathbf{r})$ is the displacement correlation function of a 2D smectic. In the other direction,

$$S_2(0, z) = \begin{cases} S_z e^{-(q_0^2 t_u^2/2) \ln^2[32e^\gamma z/z^*]}, & z \gg z^*; \\ e^{-q_0^2 g^{2D}(0, z)}, & z \ll z^*, \end{cases} \quad (3.44)$$

where $S_z = e^{-q_0^2 t_u^2 C_z}$ is a constant.

2. Inter-plane Correlations

As we have just seen $S(\mathbf{r}, na)$ is zero when $n \neq 0$ if $V^u = 0$. When V^u is not zero, $S(\mathbf{r}, na)$ is not zero, and it can be calculated perturbatively in an expansion in V^u/T . Using the decomposition of Eq. (2.18) of $\mathcal{H}_{DNA}^{\text{tot}}$ in to \mathcal{H}^{SC} and \mathcal{H}^u , we can express $S(\mathbf{r}, na)$ as

$$S(\mathbf{r}, na) = \frac{\langle e^{-\mathcal{H}^u/T} e^{iq_0[u_z^n(\mathbf{r}) - u_z^0(0)]} \rangle}{\langle e^{-\mathcal{H}^u/T} \rangle}, \quad (3.45)$$

where $\langle \cdot \rangle$ signifies an average with respect to \mathcal{H}^{SC} . This expression is easily expanded in a power series in V^u/T . The evaluation of even the lowest order term in this expansion cannot be carried out analytically. In App. F, we evaluate the lowest order term in an approximation in which $K_y = 0$, $B_{uh} = 0$, and correlations in $\partial_z u_y^n(\mathbf{r})$ in different layers are ignored. The result for the Fourier transform of $S(\mathbf{r}, na)$ is

$$S(\mathbf{q}_\perp, na) = \left(\frac{\tilde{V}^u}{2T} \right)^n [S_2(\mathbf{q}_\perp)]^{n+1}, \quad (3.46)$$

where $\tilde{V}^u = V^u e^{-W_y}$ with

$$W_y = q_0^2 a^2 \langle (\partial_z u_y^n)^2 \rangle / 2 \quad (3.47)$$

and

$$S_2(\mathbf{q}_\perp) = \int \frac{d^2 q_\perp}{(2\pi)^2} e^{-i\mathbf{q}_\perp \cdot \mathbf{r}} S_2(\mathbf{r}) \quad (3.48)$$

is the Fourier transform of the two-dimensional intra-plane density correlations function of Eq. (3.42). Since the expression, Eq. (3.46), for $S(\mathbf{q}_\perp, na)$ was derived under the assumption that $K_y = 0$, $S_2(\mathbf{r})$ is strictly speaking the density correlation of an isolated 2D smectic. However, a more sophisticated variational approximation, to be presented in a separate publication [14], yields a result very similar to Eq. (3.46) for $S(\mathbf{q}_\perp, na)$ with $S_2(\mathbf{q}_\perp)$ replaced by the true intra-plane correlation function with $K_y \neq 0$ obtained by Fourier transforming $S(\mathbf{r}, 0)$ of Eq. (3.41).

Transforming $S(\mathbf{q}_\perp, na)$ back to real space, we obtain

$$S(\mathbf{r}, na) = \left(\frac{\tilde{V}^u}{2T} \right)^n \int \frac{d^2 q_\perp}{(2\pi)^2} e^{i\mathbf{q}_\perp \cdot \mathbf{r}} e^{(n+1) \ln S_2(\mathbf{q}_\perp)}. \quad (3.49)$$

The large n limit of this expression can be calculated using steepest descents. For fixed \mathbf{r} and $n \rightarrow \infty$, the result is

$$S(\mathbf{r}, na) = \frac{2\pi T}{\tilde{V}^u n \xi_x \xi_z} e^{-|n|a/\xi_y} e^{-[(x^2/\xi_x^2) + (z^2/\xi_z^2)]}, \quad (3.50)$$

where

$$\xi_\alpha^2 = \frac{1}{S_2(\mathbf{r} = 0)} \int d^2 r r_\alpha^2 S_2(\mathbf{r}) \quad (3.51)$$

for $\alpha = x, z$, and $r_\alpha = x, z$ and

$$\xi_y = a \ln \left(\frac{2T}{\tilde{V}^u S_2(\mathbf{q}_\perp = 0)} \right)^{-1}. \quad (3.52)$$

Since $S_2(\mathbf{r})$ dies off at least as fast as e^{-r} when $K_y = 0$ [9,10] and as $\exp(-\text{const.} \ln^2 r)$ when $K_y \neq 0$, the integrals in Eq. (3.51) converge, and ξ_x and ξ_z are well defined.

D. X-ray Scattering

X-ray scattering experiments probe $I(\mathbf{q}) = \langle \rho(\mathbf{q}) \rho(-\mathbf{q}) \rangle / V$, where V is the volume of the system, and $\rho(\mathbf{q})$ is the weighted sum of the DNA and membrane densities $\rho_{DNA}(\mathbf{x})$ and $\rho_{\text{mem}}(\mathbf{x})$. The total scattering intensity can thus be broken up into a DNA contribution $I_{DNA}(\mathbf{q})$, a membrane contribution $I_{\text{mem}}(\mathbf{q})$, and a DNA-membrane cross term. Scattering from the ordinary columnar phase will exhibit true Bragg peaks at $\mathbf{G}_{lm} = (0, (l + \frac{1}{2}\sigma m)k_0, mq_0)$. Here $\sigma = 0$ for a simple rectangular columnar lattice, and $\sigma = 1$ for a centered rectangular columnar lattice. Since there is no long-range positional order in the SC phase, there will be no Bragg peaks in its x-ray scattering profile. Rather there will be membrane-dominated lamellar peaks at $\mathbf{G}_{l0} = (0, lk_0, 0)$ and DNA-dominated sub-power-law peaks at \mathbf{G}_{lm} for $m \neq 0$.

The contribution of lipid membranes to the x-ray scattering intensity is

$$I_{\text{mem}}(\mathbf{q}) = \frac{1}{a} |f_{\text{mem}}(q_y)|^2 \times \sum_n e^{-iq_y na} \int d^2 r e^{-i\mathbf{q}_\perp \cdot \mathbf{r}} S_h(\mathbf{r}, na, q_y), \quad (3.53)$$

where

$$S_h(r, na, q_y) = \langle e^{-iq_y [h^n(\mathbf{r}) - h^0(0)]} \rangle = e^{-q_y^2 g_h(\mathbf{r}, na)}. \quad (3.54)$$

and $g_h(\mathbf{r}, na)$ is evaluated in Eq. (3.36). Thus, for example,

$$S_h(0, na, k_0) \sim (na)^{-\eta_h} \quad (3.55)$$

Except for some anisotropies, this yields power-law Bragg peaks that are essentially identical to those of a normal lamellar smectic.

The contribution of the DNA lattices to the x-ray scattering intensity is

$$I_{DNA}(\mathbf{q}) = \langle \rho_{DNA}(\mathbf{q}) \rho_{DNA}(-\mathbf{q}) \rangle = \frac{1}{a} \sum_{nk} |f_y^k(q_y)|^2 |\rho^{nk}|^2 e^{-iq_y na} e^{-ikq_0 z^n} \times \int d^2 r e^{-i\Delta \mathbf{q}_\perp^k \cdot \mathbf{r}} S_{yz}(\mathbf{r}, na, q_y, k), \quad (3.56)$$

where $\Delta\mathbf{q}_\perp^k = \mathbf{q}_\perp - kq_0\mathbf{e}_z$ and

$$S_{yz}(\mathbf{r}, na, q_y, k) = \langle e^{-iq_y[u_y^n(\mathbf{r}) - u_y^n(0)]} e^{-iq_0k[u_z^n(\mathbf{r}) - u_z^n(0)]} \rangle. \quad (3.57)$$

This correlation function is even more complicated to calculate than $S(\mathbf{r}, na)$ [Eq. (3.45)]. When $B_{uh} = 0$, u_y^n and u_z^n decouple, and when $k = \pm 1$ we have

$$S_{yz}(\mathbf{r}, na, q_y, k = \pm 1) = S_h(\mathbf{r}, na, q_y)S(\mathbf{r}, na), \quad (3.58)$$

where we used the fact that correlations in u_y^n are the same as those in h^n . Thus, at $\mathbf{r} = 0$, this function dies off as $n^{-\eta_h-1}e^{-na/\xi_y}$ when $q_y = k_0$.

If we ignore the $S_h(\mathbf{r}, na, q_y)$ contribution of S_{yz} (which would be justified for $B_{\text{lam}} \rightarrow \infty$) and we use the approximation of Eq. (3.49) for $S(\mathbf{r}, na)$, then the sum over n in Eq. (3.56) can be carried out exactly. The result for the dominant contribution with $k = \pm 1$ is

$$I_{DNA}(\mathbf{q}) = \frac{1}{a} S_2(\Delta\mathbf{q}_\perp^1) |f_{DNA}^1(q_y)|^2 F(\mathbf{q}), \quad (3.59)$$

where

$$F(\mathbf{q}) = \frac{1 - \left(\frac{V^u S_2(\Delta\mathbf{q}_\perp^1)}{2T}\right)^2}{1 - 2\frac{V^u S_2(\Delta\mathbf{q}_\perp^1)}{T} \cos(q_y a - \sigma\pi) + \left(\frac{V^u S_2(\Delta\mathbf{q}_\perp^1)}{2T}\right)^2}. \quad (3.60)$$

The structure function $F(\mathbf{q})$ reaches a maximum at $q_y = mk_0$ if a rectangular ($\sigma = 0$) lattice is preferred and at $q_y = (m + \frac{1}{2})k_0$ when a centered rectangular lattices ($\sigma = 1$) is preferred. At these peaks, $F(\mathbf{q})$ does not exhibit singular behavior: the function $S_2(\Delta\mathbf{q}_\perp)$ [Eq. (3.48)] entering Eq. (3.60) can be expanded in powers of $\Delta\mathbf{q}_\perp$ to all orders.

Out-of-plane lamellar fluctuations, ignored in Eqs. (3.59) and (3.60) (by assuming $B_{\text{lam}} \rightarrow \infty$), become significant when the inter-layer positional coupling V^u is weak. For example, for $V^u = 0$ and finite B_{lam} , we find using Eqs. (3.56) to (3.58),

$$I_{DNA} = \frac{1}{a} |f_{DNA}^1(q_y)|^2 \times \int d^2r e^{-\Delta\mathbf{q}_\perp^1 \cdot \mathbf{r}} S_h(\mathbf{r}, na = 0, q_y) S_2(\mathbf{r}), \quad (3.61)$$

Using Eq. (3.54), it is easy to see that $I_{DNA}(\mathbf{q})$ has a *maximum* at $q_y = 0$, $\Delta\mathbf{q}_\perp^1 = 0$ (even for infinitely thin DNA, with $f_{DNA}^1(q_y) = 1$). This peak remains at $q_y = 0$ for sufficiently weak nonzero V^u [14]. Thus, for sufficiently weak interlayer coupling, the scattering structure factor has a form resembling that of a simple rectangular lattice, with a (0, 1)-like peak at $q_y = 0$ even though the system has short-range centered rectangular order *in real space*. With increasing strength of inter-layer positional coupling, this peak will bifurcate, at a critical value of

V^u , into two $(\pm 1, 1)$ peaks at nonzero q_y [as in Fig. 2]. Such a change of the form factor is not accompanied by a thermodynamic phase transition. It is similar in character to the transition across so-called disordering line in random microemulsions [20,21] at which the wave-vector maximizing $S(\mathbf{q})$ vanishes.

IV. STABILITY OF THE SLIDING COLUMNAR PHASE

Until now, we have treated the sliding columnar phase as though it were thermodynamically stable. We will now examine conditions for this stability. In order for the SC phase to exist, it must be stable against forces that bring about registry between neighboring DNA lattices to produce the columnar phase; and it must be stable with respect to the disordering effect of dislocations that leads to a nematic lamellar phase. In this section, we will investigate these two effects. We find that the SC phase orders into the columnar phase via a roughening-like transition at a decoupling temperature T_d and that it melts to the nematic phase via a dislocation unbinding transition at a temperature T_{KT} . Thus, the SC phase can only exist in a temperature range $T_d < T < T_{KT}$, and it cannot exist at all if $T_{KT} < T_d$. We calculate T_d and T_{KT} for our nearest-neighbor model, and we find that

$$\beta = \frac{T_{KT}}{T_d} = \frac{1}{\pi^2} < 1 \quad (4.1)$$

for systems with temperature independent coupling constants. Thus $T_{KT} < T_d$, and, for our model, the SC phase is never thermodynamically stable. The introduction of competing nearest-neighbor and next-nearest-neighbor strain couplings can, however, reverse the inequality on T_{KT} and T_d and stabilize the SC phase [13]. Even when the SC phase is not thermodynamically stable, there is a range of length scales in the lamellar nematic phase in which correlation functions will exhibit SC behavior.

A. Relevance of Translational Coupling

In the sliding columnar phase, fluctuations of relative displacements $u_z^{n+1}(\mathbf{r}) - u_z^n(\mathbf{r})$ of DNA lattices in neighboring galleries grow with increasing systems size. We found in Sec. III A 2 that $\langle [u_z^{n+1}(\mathbf{r}) - u_z^n(\mathbf{r})]^2 \rangle \sim \ln L$ [See Eqs. (3.15) and (3.22)]. Due to this divergence, the translational coupling [Eq. (2.16)] may become irrelevant above a critical decoupling temperature. This result is obtained by calculating the expectation value of the translational coupling

$$\langle \mathcal{H}_n^u \rangle = -V^u \int d^2r \langle \cos[q_0(u_z^{n+1} - u_z^n + a\partial_z u_y^n)] \rangle \quad (4.2)$$

with respect to the sliding columnar Hamiltonian in (3.1). Because the cross correlation $\langle \partial_z u_y^n (u_z^{n+1} - u_z^n) \rangle$ is zero, we can evaluate this quantity exactly:

$$\langle \mathcal{H}_n^u \rangle = -V^u e^{-W_y} \int d^2 r \exp[-q_0^2 g^{(1)}(a)], \quad (4.3)$$

where $W_y = q_0^2 a^2 \langle (\partial_z u_y^n)^2 \rangle / 2$, Using the fact that $g^{(1)}(na)$ diverges logarithmically with system size [Eq. (3.22)], we find that the translational coupling scales as

$$\langle \mathcal{H}_n^u \rangle \sim -V^u e^{-W_y} L^{2-\eta_d}, \quad (4.4)$$

where

$$\eta_d = 2(q_0 l_u)^2 S_1(0) = \frac{4T}{d^2 \sqrt{BK_y}}. \quad (4.5)$$

The condition $2 - \eta_d = 0$ defines the critical decoupling temperature

$$T_d = \frac{d^2 \sqrt{BK_y}}{2}. \quad (4.6)$$

When $T < T_d$, the translational coupling scales as system size to a positive power, and V^u is relevant. In this case, the system becomes a columnar phase at the longest lengthscales with a nonzero shear modulus for shifting neighboring lattices relative to each other and long-range positional order in the yz plane. When $T > T_d$, the translational coupling scales as the system size to a negative power, and V^u is irrelevant. The system flows to the sliding columnar phase at the longest lengthscales when $T > T_d$. Thus, T_d marks the transition from the columnar phase to the SC phase as temperature is increased. This transition is of the roughening type. There is no energy cost for shifting neighboring lattices relative to each other, and thus the sliding columnar phase is positionally disordered in the yz plane. These conclusions are supported by an RG analysis to be presented in Ref. [14].

B. Dislocation unbinding

We have just seen how thermal fluctuations weaken interlayer couplings to produce the SC phase from the columnar phase. We will now consider the disordering effects of dislocations. An individual edge dislocation in a $2D$ smectic has a finite rather than a logarithmically divergent energy. As a result, there are thermally excited unbound vortex pairs at all temperatures that convert the $2D$ smectic into a $2D$ nematic at the longest lengthscales [9]. In a sliding columnar phase, each DNA smectic layer experiences an orientational ordering field from its neighbors. As a result, the energy of an individual edge dislocation in a given layer diverges logarithmically with system size, and there can be a Kosterlitz-Thouless dislocation unbinding transition. The low-temperature phase with bound dislocations is the sliding columnar phase, and the high-temperature phase with unbound dislocations is the lamellar nematic phase.

1. Dislocation Energy

The DNA smectic lattice in each layer can have edge dislocation defects in which the displacement field u_z^n undergoes a change of kd , where k is an integer, in one circuit around the defect core. If there are dislocations with integer strengths $k_{n,l}$ at positions $\mathbf{r}_{n,l}$ in layer n , then

$$\nabla_{\perp} \times \mathbf{v}^n(\mathbf{r}) = b^n(\mathbf{r}) \hat{y}, \quad (4.7)$$

where $\mathbf{v}^n(\mathbf{r}) = \nabla_{\perp} u_z^n(\mathbf{r})$ and

$$b^n(\mathbf{r}) = d \sum_l k_{n,l} \delta^2(\mathbf{r} - \mathbf{r}_{n,l}) \quad (4.8)$$

is the dislocation density in layer n .

We can now calculate the energy cost of an arbitrary assembly of edge dislocations in the sliding columnar phase using the SC Hamiltonian

$$\mathcal{H}^{\text{sc}} = \frac{1}{2} \sum_n a \int d^2 r \left[B(v_z^n)^2 + K(\partial_x v_x^n)^2 + \frac{K_y}{a^2} (v_x^n - v_x^{n+1})^2 \right] \quad (4.9)$$

written in terms of $\mathbf{v}^n(\mathbf{r}) = (v_x^n, v_z^n)$. Our strategy is to minimize this Hamiltonian subject to a nonzero dislocation density $b^n(\mathbf{r})$. As usual, the calculation is simpler in Fourier space. To transform from real space to Fourier space, we use

$$\mathbf{v}(\mathbf{q}) = \sum_n a \int d^2 r e^{-i(\mathbf{q}_{\perp} \cdot \mathbf{r} + q_y n a)} \mathbf{v}^n(\mathbf{r}), \quad (4.10)$$

$$\begin{aligned} b(\mathbf{q}) &= \sum_n a \int d^2 r e^{-i(\mathbf{q}_{\perp} \cdot \mathbf{r} + q_y n a)} b^n(\mathbf{r}) \\ &= ad \sum_{n,l} k_{n,l} e^{-i(\mathbf{q}_{\perp} \cdot \mathbf{r}_{n,l} + q_y n a)}. \end{aligned} \quad (4.11)$$

We minimize Eq. (4.9) using the Euler-Lagrange equations and find

$$v_x(\mathbf{q}) = -\frac{q_z}{q_x} \frac{B}{K(\mathbf{q})q^2} v_z(\mathbf{q}), \quad (4.12)$$

where

$$K(\mathbf{q})q^2 = Kq_x^2 + K_y q_y^2 p(q_y a). \quad (4.13)$$

We then employ the constraint, Eq. (4.7), to relate $v_z(\mathbf{q})$ to the specified dislocation density $b(\mathbf{q})$. In the final step, we insert the expressions for $\mathbf{v}(\mathbf{q})$ into the Fourier transformed version of Eq. (4.9) and find

$$E_D = \frac{B}{2} \int_{-\pi/a}^{\pi/a} \frac{dq_y}{2\pi} \int \frac{d^2 q_{\perp}}{(2\pi)^2} \frac{K(\mathbf{q})q^2 |b(\mathbf{q})|^2}{Bq_z^2 + K(\mathbf{q})q^2 q_x^2} \quad (4.14)$$

for the energy of edge dislocations in the sliding columnar phase. Also note that if we set $K_y = 0$, Eq. (4.14) reduces

to the expression for the energy cost for edge dislocations in a 2D smectic [9].

We now decompose the dislocation energy into a part that diverges with system size and a part that diverges only with the separation between defects. After we insert Eq. (4.11) into Eq. (4.14), we find

$$E_D = \frac{\sqrt{BK_y}d^2}{4\pi^2} \left[\sum_{n,n'} \sigma_n \sigma_{n'} J_{n-n'} \ln [B_{n-n'}(\Lambda_x) L_x / x^*] + \sum_{n,n',l,l'} k_{n,l} k_{n',l'} E_{n-n'}(\mathbf{r}_{n,l} - \mathbf{r}_{n',l'}) \right], \quad (4.15)$$

where $\sigma_n = \sum_l k_{n,l}$ is the total dislocation charge in the n th layer,

$$J_n = \int_0^\pi du \sqrt{u^2 p(u)} \cos nu = \frac{4}{1-4n^2}, \quad (4.16)$$

and $B_n(\Lambda_x)$ is given in Appendix G. The first term diverges logarithmically with system size. The interaction energy $E_n(\mathbf{r})$ [Eq. (4.15)], on the other hand, is written in terms of an integral that vanishes when $\mathbf{r} = 0$, and thus it diverges only with the separation between defects. In the limit of infinite system size, $J_{n-n'}$ is a positive definite matrix. The dislocation energy diverges logarithmically with system size unless the total dislocation charge in each layer is zero, i.e., $\sigma_n = 0$ for every n .

The dislocation interaction energy of Eq. (4.15),

$$E_n(\mathbf{r}) = - \int_0^\pi du \int_0^{\Lambda_x x^*} \frac{dt}{t} \sqrt{t^2 + u^2 p(u)} \cos nu \quad (4.17) \\ \times \left(1 - \cos[tx/x^*] \exp \left[-\frac{z}{z^*} t \sqrt{t^2 + u^2 p(u)} \right] \right),$$

is difficult to calculate for arbitrary separations (\mathbf{r}, na) , however, it can be calculated in the limits $x \gg x^*$, $z = 0$ and $z \gg z^*$, $x = 0$. We find that $E_n(\mathbf{r})$ scales as

$$E_n(\mathbf{r}) = -J_n \begin{cases} \ln[C_n^x(\Lambda_x)|x/x^*] & \text{if } x \gg x^* \text{ and } z = 0 \\ \ln[C_n^z(\Lambda_x)|z/z^*] & \text{if } z \gg z^* \text{ and } x = 0, \end{cases}$$

where $C_n^{x,z}(\Lambda_x)$ are numbers that depend on the layer index n and the cutoff Λ_x and are given in Appendix G. Note that the $\Lambda_x \rightarrow \infty$ limit of $E_n(\mathbf{r})$ is not well-defined. Since $E_n(r) \sim \ln r / (4n^2 - 1)$ for large r , $E_n(\mathbf{r})$ is positive for all $n > 0$ and negative for $n = 0$. As a result, like-signed dislocations in different layers *attract* each other, whereas like-signed dislocations in the same layer *repel* each other.

The attraction of like-sign dislocations in different galleries makes physical sense. The dislocation excitations of the SC phase can be viewed as closed loops carrying a single value of charge with portions of the loop passing normal to layers and portions passing parallel to layers. Those parts of the loops passing through layers give rise to layer dislocations, and those parts aligned parallel to layers cost no energy because the shear modulus is zero

[6,7]. A direction can be assigned to a loop. A loop section penetrating a layer in the upward direction gives rise to a dislocation of one sign while one penetrating in the downward direction gives rise to a dislocation of the opposite sign. As is apparent from Fig. 4, the expectation is that the lowest energy configuration of a continuous loop will penetrate nearby points in nearby layers in the same direction, i.e., that nearby dislocations in nearby layers will have the same sign. This argument is, of course, not rigorous because it is possible for dislocation lines running parallel to layers to cross to produce nearby dislocations in nearby layers of opposite sign as shown in Fig. 4(e). In fact, it is possible to construct interlayer interactions for which like sign dislocations in neighboring layers repel rather than attract.

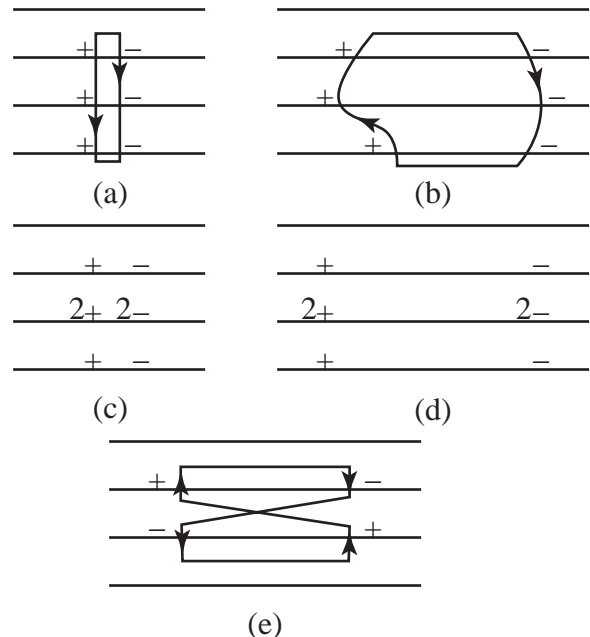


FIG. 4. (a) A sequence of closely bound dislocations in neighboring layers interpreted as a dislocation loop. (b) An unbound version of the dislocation configuration of (a), also interpreted as a dislocation loop. (c) a complex composite-dislocation pair. (d) Melted composite pair of (c). (e) Opposite sign dislocations at nearby points in neighboring layers interpreted as a crossed dislocation loop.

2. Dislocation Unbinding Temperature

In the previous section, we showed that the dislocation energy is logarithmically divergent unless there is dislocation charge neutrality in each layer. Consider now a configuration in which layer n has a single dislocation of charge σ_n (which may be zero). The free energy of such a composite dislocation configuration is, by Eq. (4.15),

$$F_D = E_D - TS_D \quad (4.18)$$

$$= \left(\frac{\sqrt{BK_y}d^2}{4\pi^2T} \sum_{n,n'} J_{n-n'} \sigma_n \sigma_{n'} - 2T \right) \ln L + \text{const..}$$

Clearly Eq. (4.18) indicates that composite dislocations pairs unbind for temperatures above the Kosterlitz-Thouless type temperature,

$$T_{KT}[\sigma_n] = \frac{\sqrt{BK_y}d^2}{8\pi^2} \sum_{n,n'} J_{n-n'} \sigma_n \sigma_{n'}. \quad (4.19)$$

If σ_n is nonzero only in layer m ($\sigma_n = \delta_{nm}$), the transition corresponds to unbinding of simple dislocations pairs within a single layer. If σ_n is nonzero in more than one layer, the transition corresponds to the unbinding of composite multilayer dislocations pairs as depicted in Fig. 4b.

We see that each configuration of dislocations $\{\sigma_n\}$ will have a different unbinding temperature. The naive expectation is that T_{KT} is lowest when there is a single dislocation in a single layer. It is, however, possible that composite dislocations might melt at a lower temperature. Hence, we define $T_{KT} = \min_{\sigma_n} T_{KT}[\sigma_n]$. Above this temperature, one of the dislocation configurations (either composite or individual) unbinds, renormalizes the compression modulus B to zero, and destroys the in-plane $2D$ smectic order of the sliding columnar phase. The lowest unbinding temperature corresponds to the configuration with the lowest $\ln L_x$ divergent energy [See Eqs. (4.19) and (4.15)]. Since $J_n < 0$ for all $n > 0$, $|J_n|$ decays with increasing layer separation, and the dislocation energy scales quadratically with the dislocation charge, the lowest energy configuration with N defects is a string of N defects of strength $+1$ with one in each layer, i.e. $\sigma_n = \sum_{p=1}^N \delta_{n,p}$. It is then straightforward to show that the lowest of these configurations is an individual defect with $N = 1$. Therefore, the dislocation unbinding temperature for the sliding columnar phase is

$$T_{KT} = \frac{d^2 \sqrt{BK_y}}{2\pi^2}. \quad (4.20)$$

The ratio of this temperature to the unbinding temperature T_d [Eq. (4.6)] yields Eq. (4.1) for $\beta = T_{KT}/T_d = 1/\pi^2$.

C. Comments on Lyotropic Systems

An interesting aspect of the present study is the transitions from the sliding to the columnar and the nematic phase we discussed above in terms of the corresponding critical temperatures: the decoupling temperature T_d [Eq. (4.6), for the columnar to sliding phase transition, and T_{KT} [Eq. (4.20)] for the sliding to nematic phase transition. In lyotropic systems of interest here [Refs. [2]- [5], temperature changes can hardly produce significant effects. Nonetheless, the above transitions can be still triggered by varying the period of DNA lattices (as

lattices described in Refs. [2]- [5]). Indeed, by previous discussions, the decoupling condition $T > T_d$, is equivalent to $\eta_d > 2$, with $\eta_d = 4T/d^2(BK_y)^{1/2}$. Thus, the decoupling transition from the columnar to sliding phase may be triggered by changing the strength of the inter-layer orientational coupling constant K_y . As evidenced clearly in experiments [4,3], the strength of inter-layer couplings significantly increases by increasing the period of DNA lattices. Thus, by the swelling these lattices, one may reach the transition in which the sliding phase changes into a columnar phase, as discussed in Sec. IV A, and, in more detail, in Ref. [14]. Finally, we emphasize that, within the simple model discussed here, there is no true sliding phase, as suggested by Eq. (4.1) that applies to systems with temperature independent coupling constants. It should be stressed however that the restriction of having temperature-independent constants is not essential for this important conclusion about the sliding phase stability. Neither it is essential whether the system is thermotropic or lyotropic in its character. Indeed, by Sec. IV A, the condition to have dislocations bound [i.e., $T < T_{KT}$] is equivalent to $\eta_{KT} > 2$, with $\eta_{KT} = d^2(BK_y)^{1/2}/\pi^2T$, for the model discussed here [Sec. II]. Note that

$$\eta_d \eta_{KT} = 4/\pi^2 < 4. \quad (4.21)$$

This relation implies that the condition for dislocations confinement ($\eta_{KT} > 2$) and the condition ($\eta_d > 2$) for sliding phase decoupling cannot be simultaneously realized. Whenever the decoupling condition is realized, $\eta_d > 2$, $\eta_{KT} = 4/\pi^2\eta_d < 2$, and dislocations will unbind. This feature turns the sliding phase into a nematic phase at long length scales. Still, at low dislocation densities (what may well be the realistic case, see Sec. V), in such a nematic phase, there is a broad range of length scales exhibiting sliding-phase correlations and other structural properties discussed in this work.

V. CHARACTERISTIC LENGTHSCALES

Whether or not sliding columnar behavior is seen in recent X-ray scattering experiments on CL-DNA complexes is still an open question [3,4]. Even though the sliding columnar phase is converted into a nematic lamellar phase at the longest lengthscales, the SC phase may exist at shorter lengthscales determined by the density of edge dislocations. Thus, CL-DNA complexes studied in recent experiments with domain sizes $L \approx 0.1\mu\text{m}$ may exhibit sliding columnar behavior. However, in the next round of experiments it will be important to prepare aligned CL-DNA samples because powder-averaging complicates the functional form of the scattering intensity and makes it difficult to identify sliding columnar behavior.

We showed in Sec. III that the density-density correlation function $S_2(\mathbf{r})$ [Eq. (3.42)] displays different functional forms depending on the magnitude of the in-plane

separation \mathbf{r} . The crossover lengthscales for the correlation function are l_x, l_z, ξ_d, x^* , and z^* . The harmonic $2D$ smectic regime is defined by $x, z < l_{x,z}$ and the nonlinear $2D$ smectic regime is defined by $x, z > l_{x,z}$, where the nonlinear lengths $l_{x,z}$ are given in Eq. (3.26). To estimate the nonlinear lengths, we must determine l_x and l_z in terms the experimentally measured quantities d and the harmonic correlation length ξ_z of Eq. (3.32). l_x and l_z can be written in terms of d and ξ_z by solving Eq. (3.32) for B_2 and using

$$K_2 = T\xi_p/2d, \quad (5.1)$$

where $\xi_p = 500\text{\AA}$ is the persistence length of DNA. Table I evaluates the nonlinear lengths for two DNA spacings of the experiments of references [2,3]. It shows that $L < l_{x,z}$ and indicates that significant departure from harmonic $2D$ smectic behavior is not expected in agreement with these experiments.

The finite length of the DNA molecules $l_{\text{DNA}} \approx 16\mu\text{m}$ introduces another crossover lengthscale. The density of DNA molecules within a given layer is $\rho = 1/dl_{\text{DNA}}$. If we assume that each free end of a DNA strand corresponds to a dislocation, then we can estimate the characteristic distance between dislocations to be

$$\xi_d = \sqrt{dl_{\text{DNA}}}. \quad (5.2)$$

This length is clearly smaller than the actual distance between dislocations because not every end of a DNA strand has to produce a dislocation: a series of DNA strands can align in a row to produce a layer of a $2D$ smectic. At lengths scales greater than ξ_d , the $2D$ smectic behaves like a nematic [9]. Using the estimate of Eq. (5.2), we find $\xi_d \approx 0.21\mu\text{m}$ and $0.30\mu\text{m}$ when $d = 28\text{\AA}$ and 55\AA , respectively. Note that $L < \xi_d$, and thus the subdomains are small enough to possess $2D$ smectic ordering.

TABLE I. The nonlinear lengths, l_x and l_z , calculated as a function of the DNA spacing d using the experimental values of the in-plane correlation length ξ_z .

Nonlinear length	$d = 28\text{\AA}$	$d = 55\text{\AA}$
l_x	$0.35\mu\text{m}$	$0.24\mu\text{m}$
l_z	$9\mu\text{m}$	$6\mu\text{m}$

We can also estimate the energy cost for creating hairpin edge dislocations within the $2D$ smectic lattices. Hairpins cause the DNA director to change by π over a lattice spacing d . The energy cost for a hairpin can be estimated from the $2D$ bending energy. If we ignore relaxation of the $2D$ smectic layers, we estimate the bending energy to be

$$\frac{E_{hp}}{2T} = \frac{\pi \xi_p}{4d}, \quad (5.3)$$

which implies that hairpins are favored on lengthscales greater than

$$\xi_{hp} = d \exp\left(\frac{E_{hp}}{2T}\right). \quad (5.4)$$

Since $\xi_{hp} \gg \xi_d > L$ throughout the experimental range in d , hairpins are not important for the current set of experiments. We do not yet have accurate estimates of x^* and z^* since the value of the orientational rigidity K_y is unknown. Scattering experiments will see sliding columnar behavior on lengthscales less than ξ_d if $x^*, z^* < \xi_d$.

VI. DISCUSSION AND CONCLUSION

In this paper, we have introduced the new sliding columnar (SC) phase of matter which may exist in layered systems composed of weakly-coupled $2D$ smectic lattices. The sliding columnar phase is characterized by weak positional but strong orientational correlations between neighboring $2D$ smectic lattices. The SC harmonic free energy contains an orientational rigidity that aligns neighboring $2D$ smectic lattices in addition to in-plane compression and bending moduli. The SC phase is characterized by a vanishing shear modulus for relative displacements of $2D$ smectic lattices. The presence of the orientational rigidity fundamentally alters the energy spectrum. In light of this, we have calculated the structural properties of the sliding columnar phase such as the SC displacement correlation function, scattering intensity, and dislocation energy.

Experimental research on layered liquid crystalline systems studied in this work is in progress [2]- [5]. Correlation peaks theoretically discussed here have been observed in a number of scattering experiments on DNA-cationic lipid complexes. Reference [4] reports DNA scattering patterns that clearly reflect the short-range centered-rectangular order depicted in Fig. 2. Reference [3], on the other hand, reports peaks in a different system at the simple rectangular lattice positions $(0, 0, \pm q_0)$ [i.e., at $(0, 1)$ peaks]. In spite of this difference in scattering data, it is likely that *both* systems have short-range centered rectangular order in *real space*. Indeed, in a strongly fluctuating disordered systems, positions of correlation peaks in q -space may not always reflect length scales and short-range order in real space. For example,

the correlation peak in q -space in random microemulsions [20,21] may occur at $q = 0$ even in situations in which real space data still show a finite structural length scale. As discussed at the end of Sec. III C, for sufficiently small coupling inter-layer positional coupling V^u/T , the scattering form factor $I_{DNA}(\mathbf{q})$ exhibits a maximum at the simple rectangular-lattice points $(0, 0, \pm q_0)$ even though the system has short-range centered rectangular order in real space. The differences between the positions of the scattering peaks in Refs. [3] and [4] may be explained by the differences in thermal disorder and/or inter-layer couplings strengths of the two systems. The interlayer correlation length reported in Ref. [4] is several times longer than that reported in Ref. [3]. The former system is stiffer and more ordered than the latter. Consequently the $(1, 1)$ and $(-1, 1)$ correlation peaks in Ref. [4] reflect the centered-rectangular order in real space depicted in Fig. 1, whereas the $(0, 1)$ peak reported in Ref. [3] reflects the merging of $(\pm 1, 1)$ peaks brought about by strong thermal fluctuations and/or sufficiently weak inter-layer couplings.

After completing this work, we learned from Joachim Rädler of experiments [22] showing a continuous variation of the DNA form factor with changing strength of inter-layer coupling V^u consistent with the change we describe above and in Sec. III D [crossover from centered rectangular scattering pattern to one resembling that of a simple rectangular lattice]. In these experiments, the variation of inter-layer positional coupling is produced by varying the period of DNA lattices in galleries. This coupling generally increases with increasing period of DNA lattices, most likely because the Coulomb interaction increases and the elastic membrane deformation increases, as suggested by electron density maps of the system [22].

ACKNOWLEDGMENTS

LG acknowledges support by Mylar Pharmaceuticals, Inc., and CSO and TCL acknowledge support from the National Science Foundation under grant DMR97-30405. We are grateful for helpful discussions with Ilya Koltover, Joachim Rädler, Cyrus Safinya, Tim Salditt, and John Toner.

APPENDIX A: DERIVATION OF EFFECTIVE HAMILTONIANS

In this appendix, we will derive the effective Hamiltonians, \mathcal{H}^{SC} [Eq. (2.19)], \mathcal{H}_z^{SC} [Eq. (3.1)], \mathcal{H}_h [Eq. (3.33)] obtained, respectively, by integrating out $h^n(\mathbf{r})$, $h^n(\mathbf{r})$ and $u_y^n(\mathbf{r})$, and $u_z^n(\mathbf{r})$ and $u_y^n(\mathbf{r})$ from $\mathcal{H} = \mathcal{H}^{\text{bend}} + \mathcal{H}^{\text{com}} + \mathcal{H}^{\text{rot}}$, which we can express in linearized form in Fourier space as

$$\tilde{\mathcal{H}} = \frac{1}{2} \int \frac{d^3 q}{(2\pi)^3} \{A_h(\mathbf{q})|h(\mathbf{q})|^2 + \sum_{\sigma} A_{\sigma}(\mathbf{q})|u_{\sigma}(\mathbf{q})|^2$$

$$- \sum_{\sigma} [\lambda_{\sigma}(\mathbf{q})u_{\sigma}(\mathbf{q})h(-\mathbf{q}) + \lambda_{\sigma}(-\mathbf{q})u_{\sigma}(-\mathbf{q})h(\mathbf{q})]\}, \quad (1.1)$$

where $\sigma = y, z$, and

$$\begin{aligned} A_h(\mathbf{q}) &= K_{3d}q_{\perp}^4 + 4(B_{3d}/a^2) \\ A_y(\mathbf{q}) &= 4(B_{3d}/a^2) + K_{2d}q_x^4 \\ A_z(\mathbf{q}) &= B_{2d}q_z^2 + K_{2d}q_x^4 + K_y q_x^2 q_y^2 p(q_y a) \\ \lambda_y(\mathbf{q}) &= (2B_{3d}/a^2) (1 + e^{-iq_y a}) \\ \lambda_z(\mathbf{q}) &= -(B_{uh}/a)iq_z (e^{-iq_y a} - 1). \end{aligned} \quad (1.2)$$

Integration over $h(\mathbf{q})$ yields

$$\begin{aligned} \tilde{\mathcal{H}}^{SC} &= \frac{1}{2} \int \frac{d^3 q}{(2\pi)^3} [A'_y(\mathbf{q})|u_y(\mathbf{q})|^2 + A'_z(\mathbf{q})|u_z(\mathbf{q})|^2 \\ &\quad - \mu(\mathbf{q})u_y(\mathbf{q})u_z(-\mathbf{q}) - \mu(-\mathbf{q})u_y(-\mathbf{q})u_z(\mathbf{q})], \end{aligned} \quad (1.3)$$

where

$$A'_{\sigma}(\mathbf{q}) = A_{\sigma}(\mathbf{q}) - \frac{|\lambda_{\sigma}(\mathbf{q})|^2}{A_h(\mathbf{q})} \quad (1.4)$$

$$\mu(\mathbf{q}) = \frac{\lambda_y(\mathbf{q})\lambda_z(-\mathbf{q})}{A_h(\mathbf{q})}. \quad (1.5)$$

In the small \mathbf{q}_{\perp} limit, these expressions reduce to

$$A'_y(\mathbf{q}) = (B_{3d}/a^2)2(1 - \cos q_y a) + K^{\alpha\beta} q_{\alpha}^2 q_{\beta}^2 \quad (1.6)$$

$$\begin{aligned} A'_z(\mathbf{q}) &= B_{2d}q_z^2 - \frac{B_{uh}^2}{4B_{3d}} q_z^2 2(1 - \cos q_y a) + K_{2d}q_x^4 \\ &\quad + K_y q_x^2 q_y^2 p(q_y a) \end{aligned} \quad (1.7)$$

$$\mu(\mathbf{q}) = -(B_{uh}/a)q_z \sin q_y a, \quad (1.8)$$

where $K^{\alpha\beta}$ is the bending rigidity tensor of Eq. (2.21). Fourier transformation of Eq. (1.3) back to real space using the low- \mathbf{q}_{\perp} form of $A_y(\mathbf{q})$, $A_z(\mathbf{q})$ and $\mu(\mathbf{q})$ produces the sliding phase Hamiltonian \mathcal{H}^{SC} of Eq. (2.19).

The effective Hamiltonian for u_z is obtained by integrating $\tilde{\mathcal{H}}^{SC}$ over u_y . The result is

$$\tilde{\mathcal{H}}_z^{SC} = \frac{1}{2} \int \frac{d^3 q}{(2\pi)^3} A''_z(\mathbf{q})|u_z(\mathbf{q})|^2, \quad (1.9)$$

where

$$A''_z(\mathbf{q}) = A'_z(\mathbf{q}) - \frac{|\mu(\mathbf{q})|^2}{A'_y(\mathbf{q})}. \quad (1.10)$$

In the $\mathbf{q}_{\perp} \rightarrow 0$ limit, $A''_z(\mathbf{q})$ becomes

$$\begin{aligned} A''_z(\mathbf{q}) &\rightarrow q_z^2 \left[B_{2d} - \frac{B_{uh}^2}{4B_{3d}} 2(1 - \cos q_y a) \right. \\ &\quad \left. - \frac{B_{uh}^2}{B_{3d}} \frac{\sin^2 q_y a}{2(1 - \cos q_y a)} \right] \end{aligned} \quad (1.11)$$

$$\begin{aligned} &+ K_y q_x^2 q_y^2 p(q_y a) + K_{2d}q_x^4 \\ &= q_z^2 \left(B_{2d} - \frac{B_{uh}^2}{B_{3d}} \right) + K_{2d}q_x^4 \\ &+ K_y q_x^2 q_y^2 p(q_y a) \end{aligned} \quad (1.12)$$

where we used the identity

$$1 - \cos \phi + \frac{\sin^2 \phi}{1 - \cos \phi} = 2 \quad (1.13)$$

to obtain Eq. (1.12) Transformation of $\tilde{\mathcal{H}}_z^{SC}$ to real space using the low \mathbf{q}_\perp form of A''_z produces \mathcal{H}_z^{SC} of Eq. (3.1). The absence of any q_y dependence in the coefficient of q_z^2 in $A''_z(\mathbf{q})$ can be traced the equality $B_{uh}^2/B_{3d} = 4B_{zz}$ [Eq. (2.20)] that results from integrating out h^n from the original model. Effective Hamiltonians for $h^n(\mathbf{r})$ and $u_y^n(\mathbf{r})$ can be obtained by respectively integrating out u_y^n and u_z^n from \mathcal{H}^{tot} and u_z^n from \mathcal{H}^{SC} . The results are

$$\mathcal{H}_h^{SC} = \frac{1}{2} \int \frac{d^3 q}{(2\pi)^3} A''_h(\mathbf{q}) |h(\mathbf{q})|^2 \quad (1.14)$$

$$\mathcal{H}_y^{SC} = \frac{1}{2} \int \frac{d^3 q}{(2\pi)^3} A''_y(\mathbf{q}) |u_y(\mathbf{q})|^2. \quad (1.15)$$

where

$$A''_h(\mathbf{q}) = A_h(\mathbf{q}) - \frac{|\lambda_z(\mathbf{q})|^2}{A_z(\mathbf{q})} - \frac{|\lambda_y(\mathbf{q})|^2}{A_y(\mathbf{q})} \quad (1.16)$$

$$A''_y(\mathbf{q}) = A_y(\mathbf{q}) - \frac{|\lambda_y(\mathbf{q})|^2}{A_h(\mathbf{q}) - |\lambda_z(\mathbf{q})|^2/A_z(\mathbf{q})}. \quad (1.17)$$

In the limit $\mathbf{q}_\perp \rightarrow 0$ with $q_x^2 \ll (B_{2d}a^2/K_y)q_z^2$, both of these Hamiltonian reduce to \mathcal{H}_h in Eq. (3.33).

APPENDIX B: CALCULATION OF $\langle (u_z^n)^2 \rangle$

In this Appendix, the expression for the sliding columnar displacement fluctuations given in (3.19) is derived. To do this, we evaluate the integral of the the Fourier transformed SC correlator $G_{zz}(\mathbf{q})$ over all q -space:

$$\langle (u_z^n)^2 \rangle = \int \frac{d^3 q}{(2\pi)^3} \frac{T}{Bq_z^2 + Kq_x^4 + K_y q_x^2 q_y^2 p(q_y a)}, \quad (2.1)$$

where $p(u) = 2(1 - \cos u)/u^2$. The fluctuations diverge at small wavenumbers $\mathbf{q} \sim 1/L$, where L is the system size. To calculate how the fluctuations scale with L_x , we set $L_z \rightarrow \infty$ and $L_y \sim L_x$. Note that the SC form for $G_{zz}(\mathbf{q})$ is valid only when $L_x \gg x^*$, where $x^* = a/\mu_y$ and $\mu_y = \sqrt{K_y/K}$. The first step in the calculation is to perform the integration over q_z with $\Lambda_z \rightarrow \infty$ and then use the fact that $G_{zz}(\mathbf{q})$ is an even function of \mathbf{q} so that the remaining integrals run over only positive q_x and q_y . Note that taking the $\Lambda_z \rightarrow \infty$ limit does not alter $q_{x,y} \rightarrow 0$ divergences. The resulting expression

$$\langle (u_z^n)^2 \rangle = \frac{T}{2\pi^2 \sqrt{BK}} \int_{L_x^{-1}}^{\Lambda_x} \frac{dq_x}{q_x} \int_{L_y^{-1}}^{\Lambda_y} dq_y \frac{1}{\sqrt{q_x^2 + \mu_y^2 q_y^2 p(q_y a)}},$$

where $\Lambda_y = \pi/a$, is made dimensionless by changing variables to $v = q_x x^*$ and $w = q_y a$. The $\ln^2 L_x$ divergence

of the displacement fluctuations can be seen immediately by looking at the $q_{x,y} \rightarrow 0$ limit of this expression.

The SC displacement fluctuations can be written as the sum of a continuum term I_c that does not depend on $p(w)$ and discrete term I_d that does depend on $p(w)$.

$$\langle (u_z^n)^2 \rangle \equiv \frac{T}{2\pi^2 \sqrt{BK_y}} [I_c + I_d], \quad (2.2)$$

where I_c and I_d are defined by

$$I_c = \int_{x^* L_x^{-1}}^{\Lambda_x x^*} \frac{dv}{v} \int_{a L_y^{-1}}^{a \Lambda_y} \frac{dw}{\sqrt{v^2 + w^2}}$$

$$I_d = \int_{x^* L_x^{-1}}^{\Lambda_x x^*} \frac{dv}{v} \int_{a L_y^{-1}}^{a \Lambda_y} dw \left[\frac{1}{\sqrt{v^2 + w^2 p(w)}} - \frac{1}{\sqrt{v^2 + w^2}} \right].$$

We first focus on the continuum contribution I_c . The integral over w is straightforward;

$$I_c = \int_{x^* L_x^{-1}}^{\Lambda_x x^*} \frac{dv}{v} [f(\Lambda_y a, v) - f(L_y^{-1} a, v)] \quad (2.3)$$

$$\equiv I_c^{(1)} - I_c^{(2)},$$

where

$$f(x, v) = \ln \left[x + \sqrt{x^2 + v^2} \right]. \quad (2.4)$$

The integral over v in $I_c^{(1)}$ can be evaluated by separating the function

$$f(\Lambda_y a, v) = \ln[2\Lambda_y a] + \ln \left[\frac{1}{2} + \frac{1}{2} \sqrt{1 + (v/\Lambda_y a)^2} \right],$$

into a constant term and a term that is well-behaved at small v . We then insert this expression into (2.3) and find that

$$I_c^{(1)} = \ln[2\Lambda_y a] \ln[\Lambda_x L_x] \quad (2.5)$$

$$+ \int_{x^* L_x^{-1}}^{\Lambda_x x^*} \frac{dv}{v} \ln \left[\frac{1}{2} + \frac{1}{2} \sqrt{1 + (v/\Lambda_y a)^2} \right].$$

The first term diverges with system size L_x , and the second term is nondivergent. $f(aL_y^{-1}, v)$ can also be separated into a constant term and a term that depends on v . We then integrate $f(aL_y^{-1}, v)$ over v to find

$$I_c^{(2)} = \ln[2aL_y^{-1}] \ln[\Lambda_x L_x] \quad (2.6)$$

$$+ \int_{x^* L_x^{-1}}^{\Lambda_x x^*} \frac{dv}{v} \ln \left[\frac{1}{2} + \frac{1}{2} \sqrt{1 + \left(\frac{L_y v}{a} \right)^2} \right].$$

The L_y dependence in the integrand of the second term can be moved to limits of the integral by changing variables to $s = L_y v/a$. In contrast to the previous expression for $I_c^{(1)}$ in (2.5), the large s part of the integral in (2.6) diverges with system size. The divergence can be

isolated by adding and subtracting $\ln[s/2]/s$. The resulting expression,

$$I_c^{(2)} = \ln[2aL_y^{-1}] \ln[\Lambda_x L_x] + \frac{1}{2} \ln^2 \left[\frac{\Lambda_x L_y}{2\mu_y} \right] - \frac{1}{2} \ln^2 \left[\frac{L_y}{2\mu_y L_x} \right] + \int_{L_y/L_x \mu_y}^{\Lambda_x L_y / \mu_y} \frac{ds}{s} \left(\ln \left[\frac{1}{2} + \frac{1}{2} \sqrt{1+s^2} \right] - \ln[s/2] \right),$$

has two terms that diverge and two terms that do not diverge with system size. Note that $L_y/L_x \mu_y$ is $\mathcal{O}(1)$ since $L_x \sim L_y$. We then subtract $I_c^{(2)}$ from $I_c^{(1)}$, drop the nondivergent terms, and set $L_y = L_x$ to obtain

$$I_c = \ln[\Lambda_x L_x] \ln[\Lambda_y L_y] - \frac{1}{2} \ln^2 \left[\frac{\Lambda_x L_y}{2\mu_y} \right] = \frac{1}{2} \ln^2 [2\mu_y \Lambda_y L_x]$$

for the continuum contribution to the displacement fluctuations.

The discrete contribution is obtained by evaluating

$$I_d = \int_{x^* L_x^{-1}}^{\Lambda_x x^*} \frac{dv}{v} F(v), \quad (2.7)$$

where

$$F(v) = \int_0^\pi dw \left[\frac{1}{\sqrt{v^2 + w^2 p(w)}} - \frac{1}{\sqrt{v^2 + w^2}} \right]. \quad (2.8)$$

In the definition of $F(v)$, we can take the lower limit to zero since the small w part of integral is well-behaved. In contrast to the continuum term, the discrete term diverges logarithmically with system size. To see this, we expand $F(v)$ around $v = 0$ and find $F(v) \approx F(0) + av^2 + \mathcal{O}(v^4)$, where $F(0) = \ln[4/\pi]$ and a is a constant. Thus, $I_d = \ln[4/\pi] \ln[\Lambda_x L_x]$ plus terms that do not diverge with system size. To make the argument of the \ln term in I_d match the \ln^2 term in I_c , we add and subtract the constant $\ln[4/\pi] \ln[2\mu_y \Lambda_y / \Lambda_x]$ to find

$$I_d = \ln[4/\pi] \ln[2\mu_y \Lambda_y L_x]. \quad (2.9)$$

We then add I_c and I_d and find the following expression for the displacement fluctuations in the limit $L_z \rightarrow \infty$ and $L_x \sim L_y$:

$$\langle (u_z^n)^2 \rangle = l_u^2 \ln^2 [8L_x/x^*]. \quad (2.10)$$

APPENDIX C: CALCULATION OF $g^{(1)}(na)$

In this appendix, we calculate the divergent part of the position correlation function $g^{(1)}(na)$ in (3.22). We perform the q_z integration, switch to dimensionless variables, and find

$$g^{(1)}(na) = 2l_u^2 \left[\int_{x^* L_x^{-1}}^{\Lambda_x x^*} \frac{dt}{t} S_n(t) + \bar{A}_n(\Lambda_x, \Lambda_z) \right], \quad (3.1)$$

where $S_n(t)$ was defined previously in (3.23) and

$$\bar{A}_n(\Lambda_x, \Lambda_z) = - \int_0^{\Lambda_x x^*} \frac{dt}{t} \int_0^\pi du \frac{1 - \cos nu}{\sqrt{t^2 + u^2 p(u)}} \times \left(1 - \frac{2}{\pi} \arctan \left[\frac{\Lambda_z z^*}{t \sqrt{t^2 + u^2 p(u)}} \right] \right). \quad (3.2)$$

Note that the integral defining $\bar{A}_n(\Lambda_x, \Lambda_z)$ does not have an infrared divergence as $t \rightarrow 0$ ($L_x \rightarrow \infty$), and thus it is a well-defined number. In the final step, we isolate the $\ln L_x$ divergence in the first term of (3.1) to find

$$g^{(1)}(na) = 2l_u^2 S_n(0) \ln [A_n(\Lambda_x, \Lambda_z) L_x/x^*], \quad (3.3)$$

where

$$A_n(\Lambda_x, \Lambda_z) = \exp[c_n^{(1)} + c_n^{(2)}(\Lambda_x) + c_n^{(3)}(\Lambda_x, \Lambda_z)] \quad (3.4)$$

depends on the layer index n and the ultraviolet cutoffs with

$$c_n^{(1)} = \int_0^1 \frac{dt}{t} \left[\frac{S_n(t)}{S_n(0)} - 1 \right], \quad (3.5)$$

$$c_n^{(2)}(\Lambda_x) = \int_1^{\Lambda_x x^*} \frac{dt}{t} \frac{S_n(t)}{S_n(0)} \quad (3.6)$$

$$c_n^{(3)}(\Lambda_x, \Lambda_z) = \frac{\bar{A}_n(\Lambda_x, \Lambda_z)}{S_n(0)}. \quad (3.7)$$

Note that $A_n(\Lambda_x, \Lambda_z)$ is well-defined in the limit $\Lambda_{x,z} \rightarrow \infty$.

APPENDIX D: CALCULATION $g^{(2)}(\mathbf{r})$

In this Appendix, we evaluate the SC position correlation function

$$g^{(2)}(\mathbf{r}) = \frac{1}{2} \langle [u_z^0(\mathbf{r}) - u_z^0(0)]^2 \rangle \quad (4.1)$$

between two DNA strands located in layer $n = 0$ and separated by \mathbf{r} in the xz plane. For general separations, $g^{(2)}(\mathbf{r})$ cannot be expressed in closed form. The aim of this Appendix is to calculate $g^{(2)}(\mathbf{r})$ along the special directions $z = 0$, $x \gg x^*$ and $x = 0$, $z \gg z^*$.

1. Large x , Small z Limit

The following expression for $g^{(2)}(x, 0)$ is obtained by setting z to zero in (3.16):

$$g^{(2)}(x, 0) = T \int \frac{d^3 q}{(2\pi)^3} \frac{1 - \cos(q_x x)}{Bq_z^2 + Kq_x^4 + K_y q_x^2 q_y^2 p(q_y a)}. \quad (4.2)$$

The first step in the derivation of $g^{(2)}(x, 0)$ is to perform the integration over q_z with $\Lambda_z \rightarrow \infty$. The q_z integration yields

$$g^{(2)}(x, 0) = \frac{T}{2\pi^2 \sqrt{BK_y}} I(x, \Lambda_x), \quad (4.3)$$

where

$$I(x, \Lambda_x) = \int_0^{\Lambda_x} dq_x \frac{1 - \cos(q_x x)}{q_x} \int_0^{\pi/x^*} \frac{dq_y}{\sqrt{q_x^2 + q_y^2 p(q_y x^*)}}.$$

We then decompose $I(x, \Lambda_x) \equiv I_c(x, \Lambda_x) + I_d(x, \Lambda_x)$ into continuum and discrete contributions as we did previously in Appendix B, where

$$I_c(x, \Lambda_x) = \int_0^{\Lambda_x} dq_x \frac{1 - \cos(q_x x)}{q_x} \int_0^{\pi/x^*} \frac{dq_y}{\sqrt{q_x^2 + q_y^2}}$$

$$I_d(x, \Lambda_x) = \int_0^{\Lambda_x} dq_x \frac{1 - \cos(q_x x)}{q_x} \int_0^{\pi/x^*} dq_y \left[\frac{1}{\sqrt{q_x^2 + q_y^2 p(q_y x^*)}} - \frac{1}{\sqrt{q_x^2 + q_y^2}} \right].$$

Since the $\Lambda_x \rightarrow \infty$ limit is well-defined, we calculate $I_c(x) \equiv I_c(x, \infty)$ and $I_d(x) \equiv I_d(x, \infty)$ and drop terms that depend on the finite ultraviolet cutoff.

To calculate the continuum contribution, we first set $q_x = uq_y$ and then $v = q_y x$. These changes of variables yield

$$I_c(x) = \int_0^{\pi x/x^*} \frac{dv}{v} K(v), \quad (4.4)$$

where

$$K(v) = \int_0^\infty du \frac{1 - \cos(uv)}{u \sqrt{1 + u^2}}. \quad (4.5)$$

The strategy for calculating the $\ln^2 x$ term in $I_c(x)$ is to isolate the part of $K(v)$ that scales as $\ln v$ for large v . To this end, we write

$$K(v) = \int_0^1 \frac{du}{u} [1 - \cos(uv)] + \int_1^\infty \frac{du}{u} \frac{1 - \cos(uv)}{\sqrt{1 + u^2}} + \int_0^1 \frac{du}{u} [1 - \cos(uv)] \left[\frac{1}{\sqrt{1 + u^2}} - 1 \right]. \quad (4.6)$$

It is obvious that only the first term has the correct scaling; the remaining terms in $K(v)$ are then separated into constants and functions of v that are well-behaved either as $v \rightarrow 0$ or $v \rightarrow \infty$. This partitioning leads to

$$K(v) = \ln(Bv) + \tilde{K}(v), \quad (4.7)$$

where $B = 2e^\gamma$, γ is Euler's constant, and

$$\tilde{K}(v) = \int_v^\infty du \frac{\cos u}{u} - \int_1^\infty \frac{du}{u} \frac{\cos(uv)}{\sqrt{1 + u^2}} - \int_0^1 du \frac{\cos(uv)}{u} \left[\frac{1}{\sqrt{1 + u^2}} - 1 \right] \quad (4.8)$$

scales as $1/v^2$ for large v .

We then insert $K(v)$ into (4.4) and break the integral over v into small- and large- v parts to obtain

$$I_c(x) = \int_0^1 \frac{dv}{v} K(v) + \int_1^{\pi x/x^*} \frac{dv}{v} \ln[Bv] + \int_1^{\pi x/x^*} \frac{dv}{v} \tilde{K}(v). \quad (4.9)$$

Next, we evaluate the integral over v in the second term, collect constants, and find

$$I_c(x) = \frac{1}{2} \ln^2[2e^\gamma \pi x/x^*] + A_x, \quad (4.10)$$

where

$$A_x = -\frac{1}{2} \ln^2[2e^\gamma] + \int_0^1 \frac{dv}{v} K(v) + \int_1^\infty \frac{dv}{v} \tilde{K}(v). \quad (4.11)$$

The second and third terms in A_x are finite since $K(v)$ scales as v^2 for small v in the former and there is phase cancellation from the $\cos(uv)$ factor at large v in the later.

We will now calculate the discrete contribution to $g^{(2)}(x, 0)$. The first step is to rewrite $I_d(x)$ in dimensionless form:

$$I_d(x) = \int_0^{\Lambda_x x^*} \frac{dv}{v} [1 - \cos(vx/x^*)] F(v), \quad (4.12)$$

where $F(v)$ was defined previously in (2.8). We next break the integral over v into small- and large- v parts and take the $x \gg x^*$ and $\Lambda_x \rightarrow \infty$ limits to obtain

$$I_d(x) = F(0) \int_0^1 \frac{dv}{v} [1 - \cos(vx/x^*)] + \int_1^\infty \frac{dv}{v} F(v) + \int_0^1 \frac{dv}{v} [F(v) - F(0)]. \quad (4.13)$$

Note that taking the $x \gg x^*$ limit removed the $\cos(vx/x^*)$ terms from the last two terms in (4.13) due to phase cancellations. It is again obvious that the first term scales logarithmically with x/x^* , and thus

$$I_d(x) = \ln[4/\pi] \ln \left[e^\gamma \frac{x}{x^*} \right] + B_x, \quad (4.14)$$

where

$$B_x = \int_0^1 \frac{dv}{v} [F(v) - F(0)] + \int_1^\infty \frac{dv}{v} F(v) \quad (4.15)$$

is a constant. The last step in the calculation of $g(x, 0)$ is to add the continuum and discrete terms, $I_c(x)$ and $I_d(x)$. The final result is

$$g^{(2)}(x, 0) = l_u^2 \left(\ln^2 \left[8e^\gamma \frac{x}{x^*} \right] + C_x \right), \quad (4.16)$$

where $C_x = 2(A_x + B_x) - \ln^2[4/\pi] - 2\ln[4/\pi]\ln[2\pi]$. A_x and B_x are computed later in this appendix, see Eqs. (4.34) and (4.35). By using these equations, we eventually find that C_x in Eq. (4.16) vanishes; $C_x = 0$.

2. Large z , Small x Limit

The calculation of $g^{(2)}(0, z)$ is similar to the calculation of $g^{(2)}(x, 0)$. The expression for $g^{(2)}(0, z)$ is obtained by setting x to zero in (3.16). The first step in the calculation is to perform the integration over q_z with $\Lambda_z \rightarrow \infty$ which yields

$$g^{(2)}(0, z) = \frac{T}{2\pi^2 \sqrt{BK_y}} I(z, \Lambda_x), \quad (4.17)$$

where

$$I(z, \Lambda_x) = \int_0^{\Lambda_x} \frac{dq_x}{q_x} \int_0^{\pi/q_x} dq_y \frac{1 - e^{-z\lambda q_x \sqrt{q_x^2 + q_y^2 p(q_y x^*)}}}{\sqrt{q_x^2 + q_y^2 p(q_y x^*)}}.$$

In what follows, we set $\Lambda_x \rightarrow \infty$, drop terms that depend on the finite ultraviolet cutoff, and define $I(z) \equiv I(z, \infty)$. The second step is to change variables to $u = q_x/q_y$ and $v = \lambda z q_y^2$ and decompose $I(z) \equiv I_c(z) + I_d(z)$ into continuum and discrete terms, where

$$I_c(z) = \frac{1}{2} \int_0^\tau \frac{dv}{v} \int_0^\infty du \frac{1 - e^{-vu\sqrt{1+u^2}}}{u\sqrt{1+u^2}} \quad (4.18)$$

$$I_d(z) = \int_0^\infty \frac{dv}{v} [F(v, 0) - F(v, vz/z^*)], \quad (4.19)$$

with $\tau = \pi^2 z/z^*$, $z^* = a^2/\mu_y^2 \lambda$,

$$F(v, \tau) = \int_0^\pi du \left[\frac{e^{-\tau\sqrt{v^2+u^2}p(u)}}{\sqrt{v^2+u^2}p(u)} - \frac{e^{-\tau\sqrt{v^2+u^2}}}{\sqrt{v^2+u^2}} \right], \quad (4.20)$$

and $F(v, 0)$ is equivalent to $F(v)$ defined in Eq. (2.8).

We first focus on the continuum contribution to $g^{(2)}(z, 0)$. The integral over v in $I_c(z)$ can be broken into small- and large- v parts,

$$I_c(z) = \frac{1}{2} \int_0^1 \frac{dv}{v} J(v) + \frac{1}{2} \int_1^{\pi^2 z/z^*} \frac{dv}{v} J(v), \quad (4.21)$$

where

$$J(v) = \int_0^\infty du \frac{1 - e^{-vu\sqrt{1+u^2}}}{u\sqrt{1+u^2}}. \quad (4.22)$$

The strategy is to extract the part of $J(v)$ that scales as $\ln v$ for large v . If $J(v) \sim \ln v$ for large v , $I_c(z)$ will

scale as $\ln^2[z/z^*]$ as expected. Note that $J(v)$ scales as v^2 for small v , and thus the first term in (4.21) is a finite constant. After some algebra, we find

$$J(v) = \ln[Dv] + \tilde{J}(v), \quad (4.23)$$

where $D = 2e^\gamma$,

$$\begin{aligned} \tilde{J}(v) &= \int_{\sqrt{2}v}^\infty du \frac{e^{-u}}{u} - \int_1^\infty du \frac{e^{-vu\sqrt{1+u^2}}}{u\sqrt{1+u^2}} \\ &\quad - \int_0^1 du \frac{1 - \Phi(u)}{u\sqrt{1+u^2}} e^{-vu\sqrt{1+u^2}}, \end{aligned} \quad (4.24)$$

and

$$\Phi(u) = \frac{1 + 2u^2}{\sqrt{1+u^2}}. \quad (4.25)$$

We can now insert the expression for $J(v)$ in (4.23) into (4.21) and obtain the continuum contribution

$$I_c(z) = \frac{1}{4} \ln^2 \left[2e^\gamma \pi^2 \frac{z}{z^*} \right] + A_z, \quad (4.26)$$

where

$$\begin{aligned} A_z &= -\frac{1}{4} \ln^2 [2e^\gamma] + \frac{1}{2} \int_0^1 \frac{dv}{v} J(v) \\ &\quad + \frac{1}{2} \int_1^\infty \frac{dv}{v} \tilde{J}(v) \end{aligned} \quad (4.27)$$

is a constant. Note that $\tilde{J}(v)$ decays exponentially for large v , and thus the third term in A_z is finite.

We now concentrate on the discrete contribution to $g^{(2)}(z, 0)$. The integral over v in $I_d(z) \equiv I_d^{(1)} + I_d^{(2)}$ can also be broken into small- and large- v parts, where

$$I_d^{(1)} = \int_0^1 \frac{dv}{v} [F(v, 0) - F(v, vz/z^*)] \quad (4.28)$$

and $I_d^{(2)}$ is an identical expression except the limits on the integral over v run from one to infinity. To isolate the $\ln z$ term in $I_d^{(1)}$, we change variables to $t = vz/z^*$ and take the $z \gg z^*$ limit. In the large z limit, (4.28) becomes

$$I_d^{(1)} = F(0, 0) \ln \left[\frac{z}{z^*} \right] + \bar{B}_z + \int_0^1 \frac{dv}{v} [F(v, 0) - F(0, 0)] \quad (4.29)$$

where $F(0, 0) = \ln[4/\pi]$ and

$$\bar{B}_z = \int_0^1 \frac{dt}{t} [F(0, 0) - F(0, t)] - \int_1^\infty \frac{dt}{t} F(0, t) \quad (4.30)$$

is a constant. The large- v contribution to I_d ,

$$I_d^{(2)} = \int_1^\infty \frac{dv}{v} F(v, 0), \quad (4.31)$$

is simply a constant when $z \gg z^*$. We then collect the discrete contributions and find

$$\begin{aligned} I_d(z) &= I_d^{(1)} + I_d^{(2)}, \\ &= \ln \left[\frac{4}{\pi} \right] \ln \left[\frac{z}{z^*} \right] + B_z, \end{aligned} \quad (4.32)$$

where $B_z = \overline{B}_z + B_x$ with B_x given by Eq. (4.15).

The last step in the calculation of $g^{(2)}(0, z)$ is to add $I_c(z)$ and $I_d(z)$. The final result is

$$g^{(2)}(0, z) = l_u^2 \left(\frac{1}{2} \ln^2 \left[32e^\gamma \frac{z}{z^*} \right] + C_z \right), \quad (4.33)$$

where $C_z = 2(A_z + B_z) - 2 \ln^2[4/\pi] - 2 \ln[4/\pi] \ln[2e^\gamma \pi^2]$. A_z and B_z are calculated later in this appendix [See Eqs. (4.36) and (4.37)]. By using these equations, we find $C_z = \pi^2/8$.

3. Calculation of A_x , B_x , A_z , and B_z

In Secs. 1 and 2 of this Appendix, we anticipated that the numerical constants A_x, B_x, A_z , and B_z have the values:

$$A_x = \frac{\pi^2}{24}, \quad (4.34)$$

$$\begin{aligned} B_x &= -\frac{\pi^2}{24} + 4 \ln^2(2) \\ &\quad - [\ln(2)][\ln(\pi)] - \frac{\ln^2(\pi)}{2}, \end{aligned} \quad (4.35)$$

$$A_z = \frac{7\pi^2}{48}, \quad (4.36)$$

$$\begin{aligned} B_z &= -\frac{\pi^2}{12} + 6 \ln^2(2) + 2\gamma \ln(2) \\ &\quad - [\ln(2)][\ln(\pi)] - \gamma \ln(\pi) - \ln^2(\pi). \end{aligned} \quad (4.37)$$

In this section we outline calculations yielding Eqs. (4.34) to (4.37). We begin by deriving more explicit formulas for these constants. Thus, for A_x , we obtain, by Eqs. (4.6), (4.8), and (4.11),

$$A_x = -\frac{1}{2} \ln^2(2e^\gamma) + A_x^{(1)} + A_x^{(2)} + \gamma A_x^{(3)}, \quad (4.38)$$

with

$$\begin{aligned} A_x^{(1)} &= -\int_0^1 dv \ln(v) \frac{1 - \cos(v)}{v} \\ &\quad + \int_1^\infty dv \ln(v) \frac{\cos(v)}{v}, \end{aligned} \quad (4.39)$$

$$\begin{aligned} A_x^{(2)} &= \int_0^1 \frac{du}{u} \left[\frac{1}{\sqrt{1+u^2}} - 1 \right] \ln(u) \\ &\quad + \int_1^\infty \frac{du}{u} \frac{1}{\sqrt{1+u^2}} \ln(u), \end{aligned} \quad (4.40)$$

and

$$\begin{aligned} A_x^{(3)} &= \int_0^1 \frac{du}{u} \left[\frac{1}{\sqrt{1+u^2}} - 1 \right] \\ &\quad + \int_1^\infty \frac{du}{u} \frac{1}{\sqrt{1+u^2}}. \end{aligned} \quad (4.41)$$

Likewise, for the constant A_z , we obtain, by Eqs. (4.22), (4.24), (4.25), and (4.27),

$$\begin{aligned} A_z &= -\frac{1}{4} \ln^2(2e^\gamma) \\ &\quad + \frac{1}{2} [A_z^{(1)} + \frac{1}{8} \ln^2(2) + \frac{\gamma}{2} \ln(2)] \\ &\quad + \frac{1}{2} [A_z^{(2)} + \gamma A_z^{(3)}], \end{aligned} \quad (4.42)$$

where

$$\begin{aligned} A_z^{(1)} &= -\int_0^1 dx \ln(x) \frac{1 - e^{-x}}{x} \\ &\quad + \int_1^\infty dx \ln(x) \frac{e^{-x}}{x}, \end{aligned} \quad (4.43)$$

$$\begin{aligned} A_z^{(2)} &= \int_0^1 du \frac{1 - \Phi(u)}{u\sqrt{1+u^2}} \ln(u\sqrt{1+u^2}) \\ &\quad + \int_1^\infty du \frac{1}{u\sqrt{1+u^2}} \ln(u\sqrt{1+u^2}), \end{aligned} \quad (4.44)$$

$$\begin{aligned} A_z^{(3)} &= \int_0^1 du \frac{1 - \Phi(u)}{u\sqrt{1+u^2}} \\ &\quad + \int_1^\infty du \frac{1}{u\sqrt{1+u^2}} \end{aligned} \quad (4.45)$$

with $\Phi(u)$ defined in Eq. (4.25). We proceed to compute the integrals in Eqs. (4.38) to (4.45). Integrals (4.41) and (4.45) can be done by elementary integration methods yielding

$$A_x^{(3)} = \ln(2), \quad A_z^{(3)} = \frac{\ln(2)}{2}. \quad (4.46)$$

Other integrals are not elementary, and we outline their calculation in the following. Thus, we compute the integrals $A_x^{(1)}$ and $A_z^{(1)}$ first by showing that

$$A_x^{(1)} = A_z^{(1)} - \frac{\pi^2}{8}. \quad (4.47)$$

and, next, by showing that

$$A_z^{(1)} = \frac{1}{2} \left(\frac{d^2 \Gamma}{dz^2} \right)_{z=1}, \quad (4.48)$$

where $\Gamma(z)$ signifies the gamma function.

To obtain Eq. (4.47), consider the complex function $f(z) = e^{-z} \ln(z)/z$. In the complex $z = x + iy$ plane, $f(z)$ is analytic inside the contour C made of the following four segments: $C_1 : [z = x; \epsilon < x < R]$, $C_2 : [z =$

$Re^{i\theta}; 0 < \theta < \pi/2$], $C_3 : [z = iy; R > y > 0]$, and $C_4 : [z = \epsilon e^{i\theta}; \pi/2 > \theta > 0]$. By applying the Cauchy residue theorem to the above $f(z)$ along the contour $C = C_1 + C_2 + C_3 + C_4$ in the limit $\epsilon \rightarrow 0$ and $R \rightarrow \infty$, we directly obtain the relation (4.47) between $A_x^{(1)}$ and $A_z^{(1)}$. Next, we demonstrate Eq. (4.48) by differentiating the standard integral representation of the gamma function. This yields

$$\left(\frac{d\Gamma}{dz}\right)_{z=1} = \int_0^\infty dx \ln(x)e^{-x} = -\gamma, \quad (4.49)$$

$$\left(\frac{d^2\Gamma}{dz^2}\right)_{z=1} = \int_0^\infty dx \ln^2(x)e^{-x}. \quad (4.50)$$

We then rewrite Eq. (4.50) as,

$$\begin{aligned} \left(\frac{d^2\Gamma}{dz^2}\right)_{z=1} &= \int_0^1 dx (e^{-x} - 1) \ln^2(x) \\ &+ \int_0^1 dx \ln^2(x) + \int_1^\infty dx e^{-x} \ln^2(x) \end{aligned} \quad (4.51)$$

and integrate by parts the first integral [by writing $(e^{-x} - 1)dx = d(1 - e^{-x} - x)$, etc.] as well as the last integral [by writing $e^{-x}dx = d(-e^{-x})$, etc.]. After few elementary integrations, this yields our Eq. (4.48) which, combined with Eq. (4.47), yields values of the integrals $A_x^{(1)}$ and $A_z^{(1)}$. To complete this calculation we need also the value of the second derivative of $\Gamma(z)$ at $z = 1$ that enters Eq. (4.48). To compute it, we use a relation from the theory of the gamma function:

$$\frac{d\Gamma(z)}{dz} = \Gamma(z)\Psi(z), \quad (4.52)$$

with

$$\begin{aligned} \Psi(z) &= -\gamma + \left(1 - \frac{1}{z}\right) + \left(\frac{1}{2} - \frac{1}{z+1}\right) \\ &+ \left(\frac{1}{3} - \frac{1}{z+2}\right) + \dots; \end{aligned} \quad (4.53)$$

$\Gamma(1) = 1$, $(d\Gamma/dz)_{z=1} = \Psi(1) = -\gamma$. By differentiating Eq. (4.52),

$$\begin{aligned} \left(\frac{d^2\Gamma}{dz^2}\right)_{z=1} &= \left(\frac{d\Gamma}{dz}\right)_{z=1} \Psi(1) + \Gamma(1) \left(\frac{d\Psi}{dz}\right)_{z=1} \\ &= \gamma^2 + \left(\frac{d\Psi}{dz}\right)_{z=1}. \end{aligned} \quad (4.54)$$

The use of Eq. (4.53) to compute $d\Psi(z)/dz$ at $z = 1$ yields

$$\begin{aligned} \left(\frac{d^2\Gamma}{dz^2}\right)_{z=1} &= \gamma^2 + 1 + \frac{1}{2^2} + \frac{1}{3^2} + \frac{1}{4^2} + \dots \\ &= \gamma^2 + \frac{\pi^2}{6}. \end{aligned} \quad (4.55)$$

By Eqs. (4.55), (4.47), and (4.48), we finally obtain

$$A_x^{(1)} = \frac{\gamma^2}{2} - \frac{\pi^2}{24}, \quad A_z^{(1)} = \frac{\gamma^2}{2} + \frac{\pi^2}{12}. \quad (4.56)$$

Next, we proceed to compute the integral $A_x^{(2)}$ in Eq. (4.40). For this purpose, consider the integrals

$$\begin{aligned} A_x^{(2)}(t) &= \int_0^t \frac{du}{u} \left[\frac{1}{\sqrt{1+u^2}} - 1 \right] \ln(u) \\ &+ \int_t^\infty \frac{du}{u} \frac{1}{\sqrt{1+u^2}} \ln(u) \end{aligned} \quad (4.57)$$

$$\begin{aligned} A_x^{(3)}(t) &= \int_0^t \frac{du}{u} \left[\frac{1}{\sqrt{1+u^2}} - 1 \right] \\ &+ \int_t^\infty \frac{du}{u} \frac{1}{\sqrt{1+u^2}} \end{aligned} \quad (4.58)$$

For $t = 1$, $A_x^{(2)}(t = 1) = A_x^{(2)}$ is the desired integral, whereas $A_x^{(3)}(t = 1) = A_x^{(3)} = \ln(2)$, by (4.46). Further, by Eqs. (4.57) and (4.58), $dA_x^{(2)}(t)/dt = -\ln(t)/t$, and $dA_x^{(3)}(t)/dt = -1/t$. By integrating these relations over t ,

$$A_x^{(2)} = A_x^{(2)}(t) + \frac{\ln^2(t)}{2}, \quad (4.59)$$

$$A_x^{(3)} = A_x^{(3)}(t) + \ln(t), \quad (4.60)$$

for *any* $t > 0$. By Eqs. (4.57) to (4.60), with $t = \epsilon \rightarrow 0$,

$$A_x^{(2)} = \lim_{\epsilon \rightarrow 0} \left[\int_\epsilon^\infty \frac{du}{u} \frac{1}{\sqrt{1+u^2}} \ln(u) + \frac{\ln^2(\epsilon)}{2} \right] \quad (4.61)$$

$$A_x^{(3)} = \lim_{\epsilon \rightarrow 0} \left[\int_\epsilon^\infty \frac{du}{u} \frac{1}{\sqrt{1+u^2}} + \ln(\epsilon) \right] \quad (4.62)$$

To proceed, it is useful to form the difference

$$\Delta = A_x^{(2)} - \frac{1}{2}[A_x^{(3)}]^2. \quad (4.63)$$

Using here Eqs. (4.61) and (4.62), we find

$$\Delta = \int_0^\infty du \frac{1}{u\sqrt{1+u^2}} \int_0^u \frac{dv}{v} \left[1 - \frac{1}{\sqrt{1+v^2}} \right]. \quad (4.64)$$

The integral over v here can be done by changing $v \rightarrow t$ with $t = \ln[(\sqrt{1+v^2} + 1)/2]$. This reduces Eq. (4.64) to

$$\Delta = \int_0^\infty du \frac{1}{u\sqrt{1+u^2}} \ln\left[\frac{\sqrt{1+u^2} + 1}{2}\right]. \quad (4.65)$$

By changing variables via $u \rightarrow t$ with $t = \ln[(\sqrt{1+u^2} + 1)/2]$, we eventually obtain Δ in a form involving a well known integral,

$$\Delta = \frac{1}{2} \int_0^\infty dt \frac{t}{e^t - 1} = \frac{\pi^2}{12}. \quad (4.66)$$

By Eqs. (4.66), (4.63), and (4.46), we obtain

$$A_x^{(2)} = \frac{\pi^2}{12} + \frac{\ln^2(2)}{2}. \quad (4.67)$$

Equations (4.38), (4.46), (4.56), and (4.67) yield our final result for the constant A_x anticipated in Eq. (4.34).

Next, we compute the integral $A_z^{(2)}$ in Eq. (4.44). For this purpose, consider the integral

$$A_z^{(2)}(t) = \int_0^t du \frac{1 - \Phi(u)}{u\sqrt{1+u^2}} \ln(u\sqrt{1+u^2}) + \int_t^\infty du \frac{1}{u\sqrt{1+u^2}} \ln(u\sqrt{1+u^2}), \quad (4.68)$$

For $t = 1$, $A_z^{(2)}(t = 1) = A_z^{(2)}$ is the desired integral. It is easy to show, along the lines we used to derive Eqs. (4.59) and (4.60), that

$$A_z^{(2)} = A_z^{(2)}(t) + \frac{[\ln(t\sqrt{1+t^2})]^2}{2} - \frac{[\ln\sqrt{2}]^2}{2}, \quad (4.69)$$

for any $t > 0$. Thus, by Eqs. (4.68) and (4.69), with $t = \epsilon \rightarrow 0$,

$$A_z^{(2)} = \lim_{\epsilon \rightarrow 0} \left[\int_\epsilon^\infty du \frac{1}{u\sqrt{1+u^2}} \ln(u\sqrt{1+u^2}) + \frac{\ln^2(\epsilon)}{2} \right] - \frac{\ln^2(2)}{8}. \quad (4.70)$$

Next, by Eqs. (4.70) and (4.61),

$$A_z^{(2)} - A_x^{(2)} = \int_0^\infty du \frac{1}{u\sqrt{1+u^2}} \ln(\sqrt{1+u^2}) - \frac{\ln^2(2)}{8}. \quad (4.71)$$

By the change of variables $u \rightarrow t$, with $u = \sqrt{e^{2t} - 1}$, we find $A_z^{(2)} - A_x^{(2)} = S_1 + S_2 - \ln^2(2)/8$, where S_1 and S_2 are two well known integrals, $S_1 = \int_0^\infty dt t/(e^t + 1) = \pi^2/12$, and $S_2 = \int_0^\infty dt t/(e^{2t} - 1) = \frac{1}{4} \int_0^\infty dx x/(e^x - 1) = \frac{1}{4}(\pi^2/6)$. Thus,

$$A_z^{(2)} - A_x^{(2)} = \frac{\pi^2}{8} - \frac{\ln^2(2)}{8}. \quad (4.72)$$

By Eqs. (4.72) and (4.67),

$$A_z^{(2)} = \frac{5\pi^2}{24} + \frac{3\ln^2(2)}{8}. \quad (4.73)$$

Equations (4.42), (4.46), (4.56), and (4.73) yield our final result for the constant A_z anticipated in Eq. (4.36).

We now proceed to discuss calculations yielding the values of the numerical constants B_x and B_z quoted in Eqs. (4.35) and (4.37). For B_x , by (4.15) and (2.8), we obtain

$$B_x = \int_0^\pi dw \left[\frac{(A_x^{(3)}(t))_{t=1/w\sqrt{p(w)}}}{w\sqrt{p(w)}} - \frac{(A_x^{(3)}(t))_{t=1/w}}{w} \right]. \quad (4.74)$$

By using (4.60), i.e., $A_x^{(3)}(t) = A_x^{(3)} - \ln(t) = \ln(2) - \ln(t)$, we find

$$B_x = \left[\int_\epsilon^\pi dw \frac{\ln(2) + \ln(w\sqrt{p(w)})}{w\sqrt{p(w)}} - \int_\epsilon^\pi dw \frac{\ln(2) + \ln(w)}{w} \right]_{\epsilon \rightarrow 0}. \quad (4.75)$$

Next, in the first integral above, we change from w to $z = w\sqrt{p(w)} = 2\sin(w/2)$, whereas in the second integral we change the variable w into z . After rearranging the expression thus obtained, we find

$$B_x = \int_0^2 dz \left[\frac{1}{\sqrt{1-(z/2)^2}} - 1 \right] \frac{\ln(2) + \ln(z)}{z} - \int_2^\pi dz \frac{\ln(2) + \ln(z)}{z}. \quad (4.76)$$

For convenience, we change variables via $z \rightarrow x = z/2$ and thus obtain

$$B_x = B^{(1)} + 2\ln(2)B^{(2)} - \frac{\ln^2(\pi)}{2} - [\ln(2)][\ln(\pi)] + \frac{3\ln^2(2)}{2}, \quad (4.77)$$

with

$$B^{(1)} = \int_0^1 dx \left[\frac{1}{\sqrt{1-x^2}} - 1 \right] \ln(x), \quad (4.78)$$

and

$$B^{(2)} = \int_0^1 dx \left[\frac{1}{\sqrt{1-x^2}} - 1 \right]. \quad (4.79)$$

A similar formula can be derived for the constant $B_z = \overline{B}_z + B_x$ introduced in Sec. D 2 of this Appendix. By Eqs. (4.20) and (4.30)), we find for \overline{B}_z

$$\overline{B}_z = \left[\int_\epsilon^\pi du \frac{\gamma + \ln(u\sqrt{p(u)})}{u\sqrt{p(u)}} - \int_\epsilon^\pi du \frac{\gamma + \ln(u)}{u} \right]_{\epsilon \rightarrow 0}. \quad (4.80)$$

By treating Eq. (4.80) in exactly the same way we treated above Eq. (4.75), we eventually find

$$\overline{B}_z = B^{(1)} + [\ln(2) + \gamma]B^{(2)} + \frac{\ln^2(2)}{2} + \gamma\ln(2) - \frac{\ln^2(\pi)}{2} - \gamma\ln(\pi). \quad (4.81)$$

To complete our calculation, we need the integrals $B^{(1)}$ and $B^{(2)}$ in Eqs. (4.78) and (4.79). $B^{(2)}$, Eq. (4.79), can be calculated by elementary integration methods yielding

$$B^{(2)} = \ln(2). \quad (4.82)$$

On the other hand, the integral $B^{(1)}$, Eq. (4.78), is not elementary. As detailed below, we find

$$B^{(1)} = -\frac{\pi^2}{24} + \frac{\ln^2(2)}{2}. \quad (4.83)$$

The values of B_x and $B_z = \overline{B}_z + B_x$ quoted in Eqs. (4.35) and (4.37), directly follow from Eqs. (4.77), (4.81), (4.82), and (4.83). It remains to outline the calculation yielding the value of $B^{(1)}$ in Eq. (4.83). It is obtained by relating the integral $B^{(1)}$, Eq. (4.78), to the integral $A_x^{(2)}$, Eq. (4.40), computed in Eq. (4.67). We find that

$$B^{(1)} = -\frac{\pi^2}{8} + A_x^{(2)}, \quad (4.84)$$

To derive relation (4.84), we apply the Cauchy residue theorem to the complex function $f(z) = \ln(z)/z\sqrt{1-z^2}$ along the same contour that has been used before to derive Eq. (4.47) [see the text following Eq. (4.48)]. This yields the relation

$$\int_{\epsilon}^1 \frac{dx}{x} \frac{1}{\sqrt{1-x^2}} \ln(x) = -\frac{\pi^2}{8} + \int_{\epsilon}^{\infty} \frac{du}{u} \frac{1}{\sqrt{1+u^2}} \ln(u) + \phi(\epsilon), \quad (4.85)$$

where $\phi(\epsilon) \rightarrow 0$ as $\epsilon \rightarrow 0$. Equation (4.85) is identical to

$$\int_{\epsilon}^1 \frac{dx}{x} \left[\frac{1}{\sqrt{1-x^2}} - 1 \right] \ln(x) = -\frac{\pi^2}{8} + \int_{\epsilon}^{\infty} \frac{du}{u} \frac{1}{\sqrt{1+u^2}} \ln(u) + \frac{\ln^2(\epsilon)}{2} + \phi(\epsilon). \quad (4.86)$$

By recalling here Eq. (4.61) and taking the limit $\epsilon \rightarrow 0$ in Eq. (4.86), we eventually obtain the relation (4.84) used to compute $B^{(1)}$.

APPENDIX E: CALCULATION OF $g^{(3)}(\mathbf{r}, na)$

In this appendix, we will outline the evaluation of Eq. (3.25) for $g^{(3)}(\mathbf{r}, na) \equiv g^{(3)}(x, z, na)$. We begin with the expression, Eq. (3.17) for $g^{(3)}(\mathbf{r}, na)$. We assume the continuum limit $\Lambda_z \rightarrow \infty$ and integrate over q_z to obtain

$$g^{(3)}(\mathbf{r}, na) = 2l_u^2 \int_0^{\Lambda_x x^*} \frac{dt}{t} \int_0^{\pi} du \frac{1 - \cos(nu)}{t\sqrt{t^2 + u^2 p(u)}} \times \left[1 - \cos(tx/x^*) e^{-(tz/z^*)\sqrt{t^2 + u^2 p(u)}} \right]. \quad (5.1)$$

This expression can now be used to evaluate various limits.

1. $x \gg x^*$ and $z = 0$

From Eq. (5.1), we have

$$g^{(3)}(x, 0, na) = 2l_u^2 \int_0^{\Lambda_x x^*} \frac{dt}{t} S_n(t) [1 - \cos(tx/x^*)], \quad (5.2)$$

where $S_n(t)$, defined in Eq. (3.23), is proportional to $1/t$ for $t \gg 1$. Thus the integral in Eq. (5.2) is convergent at large t , and we can take the continuum limit $\Lambda_x \rightarrow \infty$. Thus, we have

$$\begin{aligned} g^{(3)}(x, 0, na) &= 2l_u^2 \int_0^{\infty} \frac{dt}{t} S_n(t) [1 - \cos(tx/x^*)] \\ &= 2l_u^2 \int_0^1 \frac{dt}{t} [1 - \cos(tx/x^*)] S_n(t) \\ &\quad + 2l_u^2 \int_1^{\infty} \frac{dt}{t} [1 - \cos(tx/x^*)] S_n(t) \end{aligned} \quad (5.3)$$

$$\begin{aligned} &= 2l_u^2 [\ln(x/x^*) + \gamma] S_n(0) \\ &\quad + 2l_u^2 \int_0^1 \frac{dt}{t} [1 - \cos(tx/x^*)] [S_n(t) - S_n(0)] \\ &\quad + 2l_u^2 \int_1^{\infty} \frac{dt}{t} [1 - \cos(tx/x^*)] S_n(t) \end{aligned} \quad (5.4)$$

The contributions from the $\cos(tx/x^*)$ terms in the integrals in Eq. (5.4) vanish when $x/x^* \gg 1$, leaving

$$g^{(3)}(x, 0, na) = 2l_u^2 S_n(0) \ln(D_n x/x^*), \quad (5.5)$$

where

$$D_n = e^{\gamma + c_n^{(1)} + c_n^{(2)}(\Lambda_x = \infty)} \quad (5.6)$$

with $c_n^{(1)}$ and $c_n^{(2)}(\Lambda_x)$ given, respectively, by Eqs. (3.5) and (3.6).

2. $x = 0$, $z \gg z^*$

Again, we will simplify our discussion by taking the limit $\Lambda_x \rightarrow \infty$ and integrating over q_x in Eq. (3.25) to obtain

$$g^{(3)}(0, z, na) = 2l_u^2 \int_0^{\infty} dt \int_0^{\pi} du \frac{1 - \cos(nu)}{t\sqrt{t^2 + u^2 p(u)}} \times \left[1 - e^{-(tz/z^*)\sqrt{t^2 + u^2 p(u)}} \right]. \quad (5.7)$$

Changing variables via $t = s\sqrt{u^2 p(u)}$, we obtain

$$g^{(3)}(0, z, na) = 2l_u^2 \int_0^{\pi} \frac{1 - \cos(nu)}{\sqrt{u^2 p(u)}} J[(z/z^*)u^2 p(u)], \quad (5.8)$$

where $J(v)$ is defined in Eq. (4.22). Next, using $J(v) = \ln(2e^\gamma) + \tilde{J}(v)$ [Eq. (4.23)], we obtain

$$g^{(3)}(0, z, na) = 2l_u^2 [\ln(z/z^*) + \gamma + \ln 2] \int_0^\pi du \frac{1 - \cos(nu)}{\sqrt{u^2 p(u)}} \\ + 2l_u^2 \int_0^\pi du \frac{1 - \cos(nu)}{\sqrt{u^2 p(u)}} \ln[u^2 p(u)] \\ + 2l_u^2 \int_0^\pi du \frac{1 - \cos(nu)}{\sqrt{u^2 p(u)}} \tilde{J}[(z/z^*)u^2 p(u)] \quad (5.9)$$

In the limit $z/z^* \rightarrow \infty$, $\tilde{J}[(z/z^*)u^2 p(u)]$ tends to zero for all u , and we obtain

$$g^{(3)}(0, z, na) = 2l_u^2 S_n(0) \ln(E_n z/z^*), \quad (5.10)$$

where

$$E_u = 2e^\gamma \exp \left[\frac{1}{S_n(0)} \int_0^\pi du \frac{1 - \cos(nu)}{\sqrt{u^2 p(u)}} \ln[u^2 p(u)] \right] \quad (5.11)$$

APPENDIX F: INTER-PLANE CORRELATIONS WHEN $v^u \neq 0$

In this appendix, we will derive Eq. (3.46) from the expression, Eq. (3.41) for $S(\mathbf{r}, na)$. We begin by looking at the linear term in V^u in $S(\mathbf{r}, a)$:

$$S(\mathbf{r}, a) = V^u/2T \int d^2 r_1 \langle e^{-iq_0 u_z^0(0)} \\ \times \left(e^{iq_0 [u_z^0(\mathbf{r}_1) - u_z^1(\mathbf{r}_1)]} e^{iq_0 a \partial_z u_y^1(\mathbf{r}_1)} + \text{c.c.} \right) e^{iq_0 u_z^1(\mathbf{r})} \rangle_{SC} \quad (6.1) \\ = \frac{V^u}{2T} \int d^2 r_1 \langle e^{iq_0 [u_z^1(\mathbf{r}) - u_z^1(\mathbf{r}_1)]} \\ \times e^{iq_0 [u_z^0(\mathbf{r}_1) - u_z^0(0)]} e^{iq_0 a \partial_z u_y^1(\mathbf{r}_1)} \rangle_{SC} \\ + \frac{V^u}{2T} \int d^2 r_1 \langle e^{iq_0 [u_z^1(\mathbf{r}) + u_z^1(\mathbf{r}_1)]} \\ \times e^{iq_0 [u_z^0(\mathbf{r}_1) + u_z^0(0)]} \times e^{iq_0 a \partial_z u_y^1(\mathbf{r}_1)} \rangle_{SC}, \quad (6.2)$$

where the subscript SC indicates that the averages are to be evaluated with respect to the sliding columnar Hamiltonian, \mathcal{H}^{SC} of Eq. (2.19). Since \mathcal{H}^{SC} is quadratic in $u_z^n(\mathbf{r})$ and $u_y^n(\mathbf{r})$, the averages in this equation can be performed exactly, and $S_2(\mathbf{r}, a)$ can be expressed as an exponential of correlations functions of $u_z^n(\mathbf{r})$ and $\partial_z u_y^n(\mathbf{r})$. The second term in Eq. (6.2) has terms in the exponential proportional to $-q_0^2 \langle [u_z^n(\mathbf{r})]^2 \rangle$ for $n = 0, 1$, which diverge in thermodynamic limit and cause the exponential to vanish. Thus only the first term of Eq. (6.2) survives, and we have

$$S(\mathbf{r}, a) = \frac{V^u}{2T} \int d^2 r_1 e^{-\Phi(\mathbf{r}_1, \mathbf{r})}, \quad (6.3)$$

where

$$\Phi(\mathbf{r}_1, \mathbf{r}) = \frac{1}{2} q_0^2 \langle (\tilde{u}_z^1(\mathbf{r}, \mathbf{r}_1) + \tilde{u}_z^0(\mathbf{r}_1, 0) + a \partial_z u_y^1(\mathbf{r}_1))^2 \rangle \\ = g^{(2)}(\mathbf{r} - \mathbf{r}_1, 0) + g^{(2)}(\mathbf{r}_1, 0) \\ + g^{(2)}(\mathbf{r}, a) + g^{(2)}(0, a) - g^{(2)}(\mathbf{r} - \mathbf{r}_1, a) - g^{(2)}(\mathbf{r}_1, a) \\ + \frac{1}{2} a^2 \langle [\partial_z u_y^1(\mathbf{r}_1)]^2 \rangle \\ + a \langle \partial_z u_y^1(\mathbf{r}_1) [\tilde{u}_z^1(\mathbf{r}, \mathbf{r}_1) - \tilde{u}_z^0(\mathbf{r}_1, 0)] \rangle; \quad (6.4)$$

here, $g^{(2)}(\mathbf{r}, na)$ is defined in Eq. (3.18), and

$$\tilde{u}_z^n(\mathbf{r}, \mathbf{r}') = u_z^n(\mathbf{r}) - u_z^n(\mathbf{r}'). \quad (6.5)$$

This expression is quite complex. It, however, simplifies considerably if we set $K_y = 0$ and $B_{uh} = 0$. Then $g^{(2)}(\mathbf{r}, a) = 0$, and all cross terms in $u_z^n(\mathbf{r})$ and $u_y^m(\mathbf{r}')$ vanish. In this case,

$$\Phi(\mathbf{r}_1, \mathbf{r}) = g^{(2)}(\mathbf{r} - \mathbf{r}_1) + g^{(2)}(\mathbf{r}_1) + W_y, \quad (6.6)$$

where $g^{(2)}(\mathbf{r}) = g^{(2)}(\mathbf{r}, 0)$ [See Eq. (3.18)] and $W_y = q_0^2 a^2 \langle (\partial_z u_y^n)^2 \rangle / 2$.

The generalization of Eqs. (6.3) and (6.4) to $n > 1$ is straightforward. The leading contribution to $S(\mathbf{r}, na)$ is

$$S(\mathbf{r}, na) = \left(\frac{V^u}{2T} \right)^n \int d^2 r_1 \dots d^2 r_n e^{-\Phi(\mathbf{r}_1, \dots, \mathbf{r}_n, \mathbf{r})}, \quad (6.7)$$

where

$$\Phi = \frac{1}{2} \left\langle \left(\sum_{m=0}^n \tilde{u}_z^m(\mathbf{r}_m, \mathbf{r}_{m+1}) + a \sum_{m=1}^n \partial_z u_y^m(\mathbf{r}_m) \right)^2 \right\rangle_{SC}, \quad (6.8)$$

where $\mathbf{r}_0 = 0$ and $\mathbf{r}_{n+1} = \mathbf{r}$. This function can be expressed in terms of the reduced correlation functions $g^{(2)}(\mathbf{r}, n)$ for $u_z^n(\mathbf{r})$ and correlation functions involving $\partial_z u_y^n(\mathbf{r})$. In general, it will have terms connecting all pairs of layers, and the evaluation of $S(\mathbf{r}, na)$ is highly nontrivial.

We can obtain a useful approximation by setting $K_y = 0$ to eliminate all $g^{(2)}(\mathbf{r}, na)$ for $n \neq 0$ and by setting $B_{uh} = 0$ to eliminate couplings between u_z^n and u_y^m . Even in this approximation, couplings between distant layers arise from $\langle \partial_z u_y^n(\mathbf{r}) \partial_z u_y^m(\mathbf{r}') \rangle$. This function, however, dies off rapidly with $n - m$, and we will set it equal to zero when $n \neq m$. [In another publication [14], we will use a variational procedure to calculate $S(\mathbf{r}, na)$. The form of $S(\mathbf{r}, na)$ evaluated with this procedure is very similar to that obtained using the above approximations.] With these approximations,

$$\Phi(\mathbf{r}_1, \dots, \mathbf{r}_n, \mathbf{r}) = q_0^2 \sum_{m=0}^n g^{(2)}(\mathbf{r}_m - \mathbf{r}_{m+1}) + n W_y \quad (6.9)$$

and

$$S(\mathbf{r}, na) = \frac{\tilde{V}^{u^n}}{2T} \int d^2r_1 \dots d^2r_n S_2(\mathbf{r}_1) \times S_2(\mathbf{r}_1 - \mathbf{r}_2) \dots S_2(\mathbf{r}_n - \mathbf{r}), \quad (6.10)$$

where

$$S_2(\mathbf{r}) = \langle e^{iq_0[u_z^n(\mathbf{r}) - u_z^n(0)]} \rangle \quad (6.11)$$

is the inplane density correlation function and where

$$\tilde{V}^u = V^u e^{-W_y}. \quad (6.12)$$

Fourier transforming this equation, we obtain Eq. (3.46) in the text.

APPENDIX G: INTERACTION ENERGY BETWEEN EDGE DISLOCATIONS

In this appendix, we evaluate the interaction energy $E(\mathbf{r}, na)$ between two dislocations with separation $\mathbf{x} = (\mathbf{r}, na)$ in the limits $x \gg x^*$, $z = 0$ and $z \gg z^*$, $x = 0$. To obtain the $x \gg x^*$, $z = 0$ limit, we must evaluate

$$E_n(x) = - \int_0^{\Lambda_x x^*} \frac{dt}{t} \int_0^\pi du \sqrt{t^2 + u^2 p(u)} \times \cos[nu] (1 - \cos[tx/x^*]). \quad (7.1)$$

We isolate the $\ln x$ divergence by adding and subtracting $\sqrt{u^2 p(u)}$ under the u -integral. This procedure yields

$$E_n(x) = -J_n \ln [C_n^x(\Lambda_x) |x|/x^*] \quad (7.2)$$

for $x \gg x^*$. In the above expression, $C_n^x(\Lambda_x) = e^\gamma B_n(\Lambda_x)$ with $B_n(\Lambda_x) = \Lambda_x x^* e^{\bar{B}_n(\Lambda_x)}$,

$$\bar{B}_n(\Lambda_x) = \int_0^{\Lambda_x x^*} \frac{dt}{t} \left[\frac{J_n(t)}{J_n} - 1 \right], \quad (7.3)$$

and

$$J_n(t) = \int_0^\pi du \sqrt{t^2 + u^2 p(u)} \cos nu. \quad (7.4)$$

The $z \gg z^*$, $x = 0$ limit is obtained in a similar way from

$$E_n(z) = - \int_0^{\Lambda_x x^*} \frac{dt}{t} \int_0^\pi du \sqrt{t^2 + u^2 p(u)} \times \cos[nu] \left(1 - \exp \left[-\frac{z}{z^*} t \sqrt{t^2 + u^2 p(u)} \right] \right). \quad (7.5)$$

We find that

$$E_n(z) = -J_n \ln [C_n^z(\Lambda_x) |z|/z^*] \quad (7.6)$$

scales logarithmically for $z \gg z^*$, where $C_n^z(\Lambda_x) = B_n(\Lambda_x) e^{\bar{C}_n^z(\Lambda_x)}$,

$$\bar{C}_n^z = \int_0^1 dy \left[\frac{1 - F_n(y)}{y} \right] - \int_1^\infty dy \frac{F_n(y)}{y}, \quad (7.7)$$

and

$$F_n(y) = \frac{1}{J_n} \int_0^\pi du \cos(nu) \sqrt{u^2 p(u)} \exp \left[-y \sqrt{u^2 p(u)} \right].$$

Note that $C_n^{x,z}(\Lambda_x)$ diverge with Λ_x , and thus $E_n(\mathbf{r})$ does not have a well-defined $\Lambda_x \rightarrow \infty$ limit.

* On leave from the Department of Physics, West Virginia University, Morgantown, WV 26506-6315. email: lgolub@larry.wvnet.edu.

† Current Address, Dept. of Chemistry and Biochemistry, UCLA, Los Angeles, CA 90095-1569. email: ohern@chem.ucla.edu.

- [1] P. L. Felgner, *et al.*, *Proc. Natl. Acad. Sci. USA* **84**, 7413 (1987).
- [2] J. O. Rädler, I. Koltover, T. Salditt, and C. R. Safinya, *Science* **275**, 810 (1997).
- [3] T. Salditt, I. Koltover, J.O. Rädler, and C.R. Safinya, *Phys. Rev. Lett.* **79**, 2582 (1997); T. Salditt, I. Koltover, J. O. Rädler, and C. R. Safinya. *Phys. Rev. E* **58**, 889 (1998).
- [4] F. Artzner, R. Zantl, G. Rapp, and J.O. Rädler, *Phys. Rev. Lett.* **81**, 5015 (1998); R. Zantl, F. Artzner, G. Rapp, and J.O. Rädler, *Europhys. Lett.* **90-96** (1998); *Europhys. Lett.* **45** 90 (1998).
- [5] I. Koltover, T. Salditt, J.O. Rädler, and C.R. Safinya, *Science*, **281**, 78-81 (1998).
- [6] L. Golubović and M. Golubović, *Phys. Rev. Lett.* **80**, 4341 (1998). Erratum *ibid.* **81**, 5704 (1998).
- [7] C. S. O'Hern and T. C. Lubensky, *Phys. Rev. Lett.* **80**, 4345 (1998).
- [8] S.A. Langer, A.J. Liu, and J. Toner, *Phys. Rev. Lett.* **70** 2443 (1993).
- [9] J. Toner and D.R. Nelson, *Phys. Rev. B* **23**, 316 (1981).
- [10] L. Golubović and Z.-G. Wang, *Phys. Rev. Lett.* **69**, 2535 (1992); *Phys. Rev. E* **49**, 2567 (1994).
- [11] V.A. Bloomfield, *Biopolymers* **31**, 1471 (1991); M.J. Stevens and K. Kremer, *J. Chem. Phys.* **103**, 1669 (1995); N. Gronbech-Jensen, R.J. Mashl, R.F. Bruinsma, and W.M. Gelbart, *Phys. Rev. Lett.* **78**, 2477 (1997); B.-Y. Ha and Andrea Liu, *Phys. Rev. Lett.* **79** 1289 (1997).
- [12] S. Chandrasekhar, B.K. Sadashiva, and K.A. Suresh, *Pramana* **9** 471 (1977); S. Chandrasekhar and G.S. Ranganath, *Rep. Prog. Phys.* **53** 57-84 (1990).
- [13] C. S. O'Hern, T. C. Lubensky, and J. Toner, *Phys. Rev. Lett.* **83**, 2745 (1999) and unpublished.
- [14] L. Golubović, C.S. O'Hern, T.C. Lubensky, and J. Toner (unpublished)
- [15] For a discussion of Lagrangian and Eulerian elastic variables, see P.M. Chaikin and T.C. Lubensky, *Principles of Condensed Matter Physics* (Cambridge University Press, Cambridge, 1995), Chap. 6.5.

- [16] H. Brand and H. Pleiner, *Phys. Rev. A* **24**, 2777 (1981).
- [17] C.S. O'Hern and T. C. Lubensky. *Phys. Rev. E* **58**, 5948 (1998).
- [18] N. Lei, C.R. Safinya, and R.F. Bruinsma, *J. Physique II (France)* **16**, 299-307 (1995).
- [19] Robert Holyst, *Phys. Rev. A* **42**, 7511 (1990); Robert Holyst, Douglas J. Tweet, and Larry B. Sorensen, *Phys. Rev. Lett.* **65** 2153 (1990).
- [20] K.-V. Schubert and R. Strey, *J. Chem. Phys.* **95**, 8532 (1991).
- [21] G. Gompper and M. Schick, *Phys. Rev. E.* **49**, 1478 (1994).
- [22] J. Rädler, private communication [Artzner *et al.*, unpublished]